

**THE INVESTIGATION ON FIBROUS VEINS AND THEIR HOST  
FROM MT. IDA, OUACHITA MOUNTAINS, ARKANSAS**

A Thesis

by

JAE WON CHUNG

Submitted to the Office of Graduate Studies of  
Texas A&M University  
in partial fulfillment of the requirements for the degree of

MASTER OF SCIENCE

December 2003

Major Subject: Geology

**THE INVESTIGATION ON FIBROUS VEINS AND THEIR HOST  
FROM MT. IDA, OUACHITA MOUNTAINS, ARKANSAS**

A Thesis

by

JAE WON CHUNG

Submitted to Texas A&M University  
in partial fulfillment of the requirements  
for the degree of

MASTER OF SCIENCE

Approved as to style and content by:

---

David V. Wiltschko  
(Chair of Committee)

---

Ethan Grossman  
(Member)

---

John W. Morse  
(Member)

---

Richard L. Carlson  
(Head of Department)

December 2003

Major Subject: Geology

## ABSTRACT

The Investigation on Fibrous Veins and Their Host from Mt. Ida, Ouachita

Mountains, Arkansas. (December 2003)

Jae Won Chung, B.S., Yonsei University

M.S., Seoul National University

Chair of Advisory Committee: Dr. David V. Wiltschko

I have studied syntectonic veins from shales and coarse calcareous sands of the Ordovician Womble Shale, Benton uplift, Arkansas. All veins are composed of calcite with minor quartz and trace feldspar and dolomite or high-Mg calcite in the coarser veins. All host lithologies have a pressure-solution cleavage, more closely spaced in the fine-grained shale beds. The vein internal fabrics are coarsely to finely fibered, with a strong host-rock grain size control on fiber width. The finest fibers are in veins with shale host and the coarsest in the coarse-grained calcareous sandstone. Fiber aspect ratio is inversely proportional to host grain size; more equant vein grains are found in the veins hosted in the coarse host fraction. Within one outcrop, the  $\delta^{13}\text{C}$  and  $\delta^{18}\text{O}$  compositions of the host lithologies range from 1.5 to  $-3.0$  per mil and 7.5 to  $-14.0$  per mil (VPDB), respectively. By contrast, the  $\delta^{18}\text{O}$  composition of the veins is remarkably constant ( $-13.5$  per mil) among veins of starkly different fabrics. This composition is identical to that of the coarse calcareous sandstone lithology in the outcrop. No cathodoluminescence or stable isotope zoning was observed in the veins. In addition, there were no gradients in Ca or Si in the vicinity of the veins, suggesting either that the host did not contribute these elements or that diffusion was not the rate-limiting step to

vein formation. In any case, the wide variety of veins was probably formed from meter-scale migration of fluid derived from local calcite-rich layers in calcareous sandstone.



## ACKNOWLEDGEMENTS

I would like to deeply thank my advisor, Dr. David V. Wiltschko, for his advice, encouragement, and financial support throughout this research. I am especially grateful to Dr. Ethan Grossman for discussion and analysis of the stable isotope data, and Dr. Renald Guillemette for microprobe analysis and advice. I would like to thank my committee member, Dr. John Morse, for his advice. I also want to thank Charles Stone for the geological map. I also thank Dr. Brann Johnson, Dr. Andreas Kronenberg, and Dr. Fredrick Chester for initiating my interest in tectonophysics. I acknowledge the encouragement and review of Dr. John Panian and Pablo Cervantes. I also thank the graduate students of the Center for Tectonophysics, Texas A&M University, for their friendship. I would also like to thank all sources of financial help for my research and education, Dr. Robert Popp, and Ms. Michele Beal for her official help.

## TABLE OF CONTENTS

|   | Page |
|---|------|
| ABSTRACT .....  | iii  |
| ACKNOWLEDGEMENTS .....  | v    |
| TABLE OF CONTENTS .....   | vi   |
| LIST OF FIGURES.....  | viii |
| LIST OF TABLES .....  | xii  |
| 1. INTRODUCTION.....  | 1    |
| 2. GEOLOGY.....   | 7    |
| 3. OUTCROP OBSERVATION.....   | 13   |
| 4. TEXTURES.....  | 18   |
| 5. RELATION BETWEEN MATRIX GRAIN SIZE AND VEIN FIBERS .....                       | 23   |
| 6. CHEMICAL COMPOSITION AND ZONING.....   | 28   |
| 6.1 Methods.....  | 28   |
| 6.2 Veins-in-shale.....   | 28   |
| 6.3 N7E vein.....   | 35   |
| 6.4 Cathodoluminescence (CL).....   | 40   |
| 7. ISOTOPIC COMPOSITIONS .....  | 42   |
| 7.1 Results .....   | 42   |
| 7.2 Interpretation .....  | 45   |
| 8. DISCUSSION... ..   | 48   |
| 8.1 Fractures and vein-filling fluid generation during tectonic compression ..... | 49   |
| 8.2 Mass transfer models.....   | 50   |
| 8.3 Fibrous vein formation .....  | 54   |
| 9. CONCLUSION... ..   | 56   |
| REFERENCES.....   | 57   |

|                  | Page |
|------------------|------|
| APPENDIX A ..... | 61   |
| APPENDIX B ..... | 62   |
| APPENDIX C ..... | 63   |
| VITA .....       | 65   |

## LIST OF FIGURES

| FIGURE | Page   |
|--------|--|
| 1      | a)-b) Typical textures of 'crack-seal' vein (after Ramsay, 1980) ..... 2   |
| 2      | Stratigraphic column in Paleozoic Ouachita Mountains in eastern Arkansas (after Howard and Stone, 1988). Sh: shale, Ss: Sandstone, Lm: limestone, Ch: chert, Cgl: conglomerate, and Nv: novaculite ..... 8   |
| 3      | Geological map of Ouachita Mountains (after Miser, 1959). Ouachita Mountains can be divided into four tectonic provinces from north to south: 1) Ozark uplift-Arkoma basin, 2) Frontal thrust belt-Maumello zone, 3) Benton uplift-Broken bow uplift, and 4) Southern Ouachitas ..... 9  |
| 4      | Geologic map of study area around Mt. Ida in Arkansas (after Haley and Stone, 1976). b) Geological cross section along A-A' in Figure 5a. No vertical exaggeration. Formation symbols are same as Figure 4 a). c) Restoration of cross section along A-A ..... 11  |
| 5      | a) Outcrop photograph of sample location in Womble Shale near Mt. Ida. b) N7E veins are typically found below the calcareous sandstone layers containing N45E veins, while N45E veins usually occur below shale. c) N45E veins layers are continuous with fibrous calcite veins-in-shale. Bedding-parallel quartz-calcite veins within calcareous sandstone. d) Simplified description of veins and their host rocks. Calcareous SS: calcareous sandstone, and Qtz-CC layer: quartz-calcite layer ..... 14 |

| FIGURE | Page   |
|--------|--|
| 6      | Equal area, lower hemisphere projections of poles and average plane to a) bedding of shale and calcareous sandstone, and regional fold axes and normals to thrust faults, b) veins-in-shale, c) N45E veins, and d) N7E veins. Great circle shows average orientations of bedding and veins. N = number of poles..... 17  |
| 7      | Photomicrographs of thin sections. a)-d) Veins-in-shale. e)-f) N45E veins. g)-h) N7E veins. For veins-in-shale, quartz rim is found between vein and wall rock: a) bedding normal view, b) bedding parallel view. a) Fibers are perpendicular to the median line and slightly curved towards the vein wall. c) Vein likely grows along vein-wall boundary rather than median line due to the fact that most of vein grains are continuous across the median line. d) Vein cross-cutting relationship between main vein and subvein and vein cutting by shear movement along stylolites. e) Length/width ratio of vein crystals. The Length/width ratio increases from the coarse-grained layer toward the fine-grained layer. f) Saw-tooth (serrated) texture is shown in grain boundaries. g) N7E veins consist of fibrous or blocky calcite near the vein wall and blocky quartz grains in center which are wider than calcite grains. h) Calcareous sandstone containing N7E veins is grouped into two layers: fine grained calcite-poor layer (CPL) and coarse-grained calcite-rich layer (CRL). Cc: calcite, Qtz: quartz, S: stylolites, and St: saw-tooth (serrated) texture..... 20 |
| 8      | a) Photomicrograph of thin section (AR30) showing the relationship between the matrix and N7E vein fibers. Numbers refer to the distance from an arbitrary origin on the left used to make the measurements in Fig. 9. b) Length and width of vein grains were measured parallel and normal to long axes of the grains. c)-h) Photomicrographs of vein-wall boundaries and sketches in coarse matrix layer (c-e) and fine matrix layer (f-h) ..... 24  |
| 9      | Size and shape relationships of N7E vein calcite (a-c), quartz (d) and matrix in calcareous sandstone sample AR30. All are measured versus distance along the vein. a) The length / width (L/W) ratio of vein grains versus host grain size. b) Fiber width versus host grain size. c) Vein fiber length versus vein width. In the fine matrix, the length of vein fibers is proportional to vein aperture thickness. d) Vein quartz L/W versus the matrix grain size. Quartz grains consisting of vein are mostly blocky with low L/W ratio, showing no relationship to matrix size..... 27   |

| FIGURE | Page   |
|--------|--|
| 10     | Chemical composition map of vein and host rock of shale (AR29). a) Detailed microprobe map (1mm × 1mm) and cathodoluminescence are shown in Figure 11 and Figure 17, respectively. b) Back-Scatter Electron (BSE) image. c) Calcium map. Calcium concentration is low in shale. d) Profiles (A-A' and B-B') of calcium across vein. There is no Ca gradient toward the vein. e) Si map. Quartz is present in the vein-wall boundary and the tip of the calcite vein. f) Enlarged view of vein tip area. The quartz presence in vein tip without vein calcite indicates that quartz predated calcite precipitation in vein. g)-h) Al and K distributions. The shale consists of mica and/or K-feldspar ..... 29 |
| 11     | Chemical composition map of vein and shale host rock (AR29). (a) Back-Scatter Electron (BSE) image. (b) Ca element map. n. (c) Si element map. The distribution of Si in the vein-wall boundary shows that quartz is present in the rim. (d) K element map. (e) Al element map. Si, K and Al distributions show that small grains of mica are irregularly present both within the quartz rim and the vein. (f) Profiles of Ca and Si, locations in b) and c), respectively. No gradient in either Ca or Si is apparent from the host toward the vein. .... 30  |
| 12     | Chemical profiles of vein, stylolites, and shale (AR29c). a) Thin section viewed on bedding. b) – e) element profiles along A-A' in a) of Ca, Si, Al and K, respectively. a) Ca is more enriched in the stylolite than in the shale, while Si, Al, and K are more depleted in the stylolite ..... 31   |
| 13     | Chemical composition map of vein in shale host rock of sample AR 29c. a) Back-Scatter Electron (BSE) image. b) Enlarged view of stylolites in Figure 13a reveals that stylolites consist of calcite, illite, and quartz. c) Composite map was created using 8 additive X-ray maps of Ca, Si, Al, K, Na, Mg, Fe, and Mn. shown in d)-k), respectively, Note in d) that Ca is more abundant in the stylolite ..... 33  |
| 14     | a) Compositional map of N7E vein (AR30). The map was created using 4 additive microprobe maps for Ca, Si, Al, and K. b)-d), profiles of counts for Ca along profiles A-A, B-B', and C-C', respectively; profiles are located on a). There is no significant Ca gradient toward vein. A-A' profile reveals that Calcium is more depleted in stylolites ..... 36   |

| FIGURE   | Page |
|--|------|
| 15 Ca count in N7E veins and matrix from Figure 14 (AR 30) shows that the Ca is more abundant in coarse matrix (CRL) than fine matrix (CPL).....   | 37   |
| 16 Enlarged photomicrographs (a: cross nicols and b: open nicol), and microprobe maps of N7E vein and calcareous sandstone, located on Figure 14. Composite map (c) was created using 8 adding together X-ray maps of Ca, Si, Al, K, Fe, Mg, Mn, and Na shown in d)- l), respectively..  | 38   |
| 17 Catholuminescence (CL) of two samples. a)-b) vein-in-shale located on Figure 10 a). c)-d) N7E vein located on Figure 14 a). The white horizontal bands in b) are scan rate artifacts. No zonation within the vein is visible in either sample. Vein quartz in sample AR30, indicated by the arrow in d), shows zonation and is brighter than quartz grains in the host. Qtz: quartz.  | 41   |
| 18 $\delta^{13}\text{C}$ and $\delta^{18}\text{O}$ profiles across a) a N45E vein (AR 26n), b)-c) a N7E vein (AR 23 and AR 30), d) veins-in-shale (AR 29 and AR61), e) Quartz-calcite layer (AR24). a)-c) $\delta^{13}\text{C}$ values of N45E vein and N7E vein in the calcite poor layer (CPL) are heterogeneous to their host rocks, while the $\delta^{13}\text{C}$ values of N7E in the calcite rich layer (CRL) are similar to those of enclosing host rock. The $\delta^{18}\text{O}$ values of N45E vein and N7E vein in the CPL are more depleted than those of their host rock, while the vein $\delta^{18}\text{O}$ values of N7E vein in CRL are similar to those of host rock. On figures of specimens, $\delta^{13}\text{C}$ values shown above $\delta^{18}\text{O}$ values. CC: calcite..... | 43   |
| 19 Carbon and oxygen isotopic composition of veins and their host rocks. See text for details.....   | 45   |

| FIGURE | Page  |    |
|--------|---|----|
| 20     | <p>Proposed diagrams illustrating the development of vein formations during uplifting, and carbon and oxygen stable isotopic relationship between veins and host rocks, and schematic fluid flow path. Stage 1: fractures develop in brittle calcareous sandstone during tectonic compression, while shale behaves more ductilely that restricts facture growth. Stage 2: shale was probably fractured when it was brought closer to the surface by tectonic uplifting. Stage 3: (a) N7E vein-forming solution is derived from the host rock. (b) The solution of vein-forming material flows into N45E veins and veins-in-shale and quartz-calcite layer. (c) During N45E vein precipitation, the input of lower <math>\delta^{13}\text{C}</math> from calcareous sandstone containing N45E vein leads to depleted carbon isotope values of N45E veins relative to other veins. Carbon isotope of veins-in-shale might be partially mixed with this lower <math>\delta^{13}\text{C}</math> of the calcareous sandstone containing N45E veins .....</p> | 47 |
| 21     | <p>a) Schematic effective transport distance of advection (<math>Xa</math>) vs. diffusion (<math>Xd</math>). Before <math>t_{crit}</math> (critical time defined as the time as <math>Xa=Xd</math>), diffusion is main transport mechanism of material for shorter distance. After <math>t_{crit}</math>, advection is dominant mass transfer mechanism over diffusion for longer distance. b) Plot showing dependence of critical time (<math>t_{crit}</math>) on the ratio (<math>K/\varphi</math>) of permeability to porosity of each rock layer as a function of pressure gradient (<math>\Delta P</math>).....</p>  | 52 |



**LIST OF TABLES**

| TABLE |   | Page |
|-------|---|------|
| 1     | Description of veins and their host rocks.....  | 19   |
| 2     | Values of parameters and calculated critical times ( $t_{crit}$ ) for rock layers ..... | 53   |

## 1. INTRODUCTION

Veins are evidence for transport and precipitation of mass in solution. Of the various vein types classified by internal texture, 'crack-seal' or banded fibrous veins are thought to be indicators of repeated crack opening along vein-wall contact followed by sealing (Ramsay, 1980; Etheridge et al., 1983; Fisher and Brantley, 1992). The bands of inclusions taken as diagnostic of 'crack-seal' veins are due to either separation of host minerals from the walls during the cracking phase and/or overgrowths on wall micas (Ramsay, 1980; Etheridge et al., 1983; Fisher and Brantley, 1992).

The fabrics of 'crack-seal' veins provide clues to their origin. A salient feature of 'crack-seal' veins is the existence of fibers that are subnormal to the vein walls with high length to width ratios. (Ramsay, 1980; Fig. 1). Typical fibers have widths ranging from 30  $\mu\text{m}$  to 200  $\mu\text{m}$  (e.g., Cox and Etheridge, 1983). The fibers also typically contain wall-parallel inclusion bands of silicate mineral spaced from 8  $\mu\text{m}$  to 40  $\mu\text{m}$  and are subparallel to both each other and the vein wall (Fisher and Brantley, 1992; Cox and Etheridge, 1983). Cox and Etheridge (1983) observed inclusion bands made up of mica grains 10  $\mu\text{m}$  long and less than 2  $\mu\text{m}$  wide and spaced about 10  $\mu\text{m}$  to 40  $\mu\text{m}$  from the vein wall (Cox and Etheridge, 1983). Fiber grain boundaries may be serrated with the serration steps spaced about the same distance as that of inclusion bands. Inclusion trails are sparse inclusion bands. They often may be traced to a grain of similar mineralogy on

---

This thesis follows the style and format of the Journal of Structural Geology.

the vein-host wall. Smaller crystals may define a median line in the center of the vein

(Fig. 1).

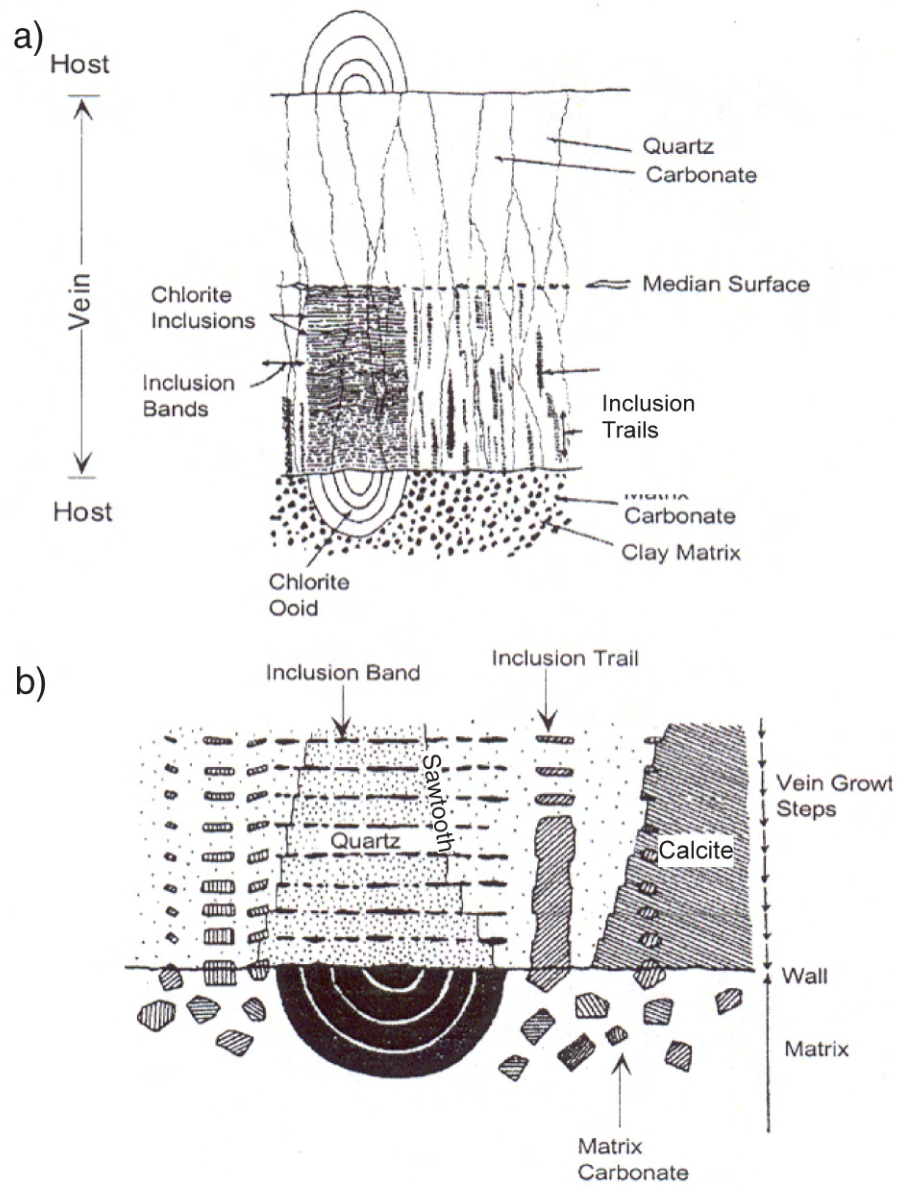


Fig. 1. a)-b) Typical textures of 'crack-seal' vein (after Ramsay, 1980).

Ramsay (1980) proposed that 'crack-seal' veins formed by episodic cracking of host rock and progressive sealing by crystal growth. The driving force for cracking has been proposed to be analogous to cyclic hydraulic fracturing (Ramsay, 1980; Etheridge et al., 1984). Wiltschko (1998) proposed reserving the crack-seal name for the mechanism and instead labeling the veins as banded veins or fibrous banded veins

Fibrous banded veins usually occur in rocks deformed under upper to subgreenschist grade metamorphism (e.g., Kirschner et al., 1995). Transport of the vein-forming minerals has variously been attributed to advection or diffusional mass transfer (e.g., Etheridge et al., 1983; Gray and Gregory, 1991; Fisher and Brantley, 1992). Based both on textural observations of veins within the Kodiak accretionary complex and mass balance calculations, Fisher and Brantley (1992) pointed out that the crack-seal mechanism is not plausible. Specifically, each episode of cracking (8  $\mu\text{m}$  wide) cannot contain enough fluid to precipitate the observed mass of quartz or calcite; the degree of saturation of quartz in pore fluids is too low to provide the observed vein materials by a crack-fill mechanism. Consequently, Fisher and Brantley (1992) proposed that diffusion from the matrix into a crack is more defensible, because this mechanism does not require large crack apertures. In support, Fisher et al. (1995) found that silica is depleted within the matrix adjacent to the Kodiak veins. Fisher and Brantley (1992), and Fisher et al. (1995) retained on hydraulic fracturing as a way to produce the quartz-mica bands. In their view, fluid for hydraulic cracking was likely derived from the basal decollement in the subduction complex by a seismic pumping. The driving force for cracking is the fluid pressure difference between the top and bottom of the fluid-filled vertical crack. The

vertical fractures will seal from bottom as they propagate upward. Each vein consists of up to thousands of episodes of fluid-filled crack passage.

Experimental and geochemical studies indicate that a mechanism whereby pressure exerted by growing crystals causes vein dilation might be a more plausible explanation (Taber, 1916a; Means and Li, 2001; Wiltschko and Morse, 2001). Taber (1916b) experimentally showed that force of crystallization during fiber growth could push apart the enclosing walls. Similarly, Means and Li (2001), and Li (2000) showed through evaporation experiments of analog materials that growing fibrous crystals could separate two ceramic blocks. They hypothesized that the morphologies and the length to width ratio of crystals in the vein are determined by the ambient humidity (a proxy for saturation state) and grain or pore size (Li, 2000). While not directly applicable to natural vein formation where evaporation plays no role, the fabrics produced are similar to those of banded fibrous veins.

The stress induced by crystal growth follows the Riecke principal (Maliva and Siever, 1988; Dewers and Ortoleva, 1990; Wiltschko and Morse, 2001):

$$P_{fc} = \left( \frac{RT}{-\Delta V} \right) \ln \Omega \quad (1)$$

where  $P_{fc}$  is pressure produced by the growing crystal,  $R$  is gas constant,  $T$  is temperature,  $\Delta V$  is volume change between a substance in solution and its precipitate, and  $\Omega$  is degree of supersaturation. Higher fluid supersaturation leads to increased stress during crystallization. In addition, Wiltschko and Morse (2001) suggested that geochemical self-

organization (e.g., Nicolis and Prigogine, 1977) can produce non-linear oscillation in vein composition, and this oscillation may make sequences of inclusion bands of quartz and mica (Wiltschko and Morse, 2001). In this model, fluid must be supersaturated and either diffusion to the vein or precipitation kinetics at the vein are the rate-limiting step(s) (Wiltschko and Morse, 2001). Fletcher and Merino (2001) further quantified the role of crystal pressure by considering how a new mineral can grow by either replacement of host mineral, or deformation of the host rock. For a spherical growing inclusion of secondary material, replacement and deformation of host would be equally likely when the viscosity of the host is given by:

$$\eta^* = 3b/(16k_B V_0^B) \quad (2)$$

where  $b$  is the radius of rock sphere containing one vein or spherical crystal,  $\eta^*$  is the critical value of surrounding host rock viscosity,  $k$  is a constant in kinetic law for precipitation/dissolution of mineral B,  $V_0$  is the specific volumes of mineral. From Eq. (2), Fletcher and Merino (2001) show that new mineral would replace host if the host rock viscosity is high ( $>\eta^*$ ), whereas growing minerals would deform the surrounding host by expansion if instead the host rock is less viscous than the material in the concretion (or vein) ( $<\eta^*$ ).

There are several features of the force of crystallization model that may lend them to observation. In this model fibrous veins can form without a precursory fracture or fluid channel. In addition, because crystallization force arises from supersaturation of the pore fluid, the force scales with the degree of supersaturation. Any process that supersaturates

the fluid will promote vein formation. The fluid pressure need not necessarily be elevated above hydrostatic.

The force of crystallization model for fibrous banded veins implies that 1) vein filling material is local or at least need not be transported far, 2) open cracks need not occur and, indeed, should be rare, and 3) fluid pressure need not be lithostatic. However, these assumptions remain untested, and veins forming different material than the country rock (e.g., calcite veins in sandstone) cannot be explained by this model. It is my goal to test some of these implications.

## 2. GEOLOGY

Samples of fibrous veins were collected from Paleozoic Womble Shale around Mt. Ida, Arkansas (Fig. 2). The study area lies within the Benton Uplift of eastern Arkansas. The Benton Uplift is the core of the Ouachita Mountains ranging from eastern Arkansas to western Oklahoma (Viele, 1973). The uplift was formed by compression due to subduction of North American beneath southern Llanoria in late Paleozoic (Houseknecht and Matthews, 1985; Lillie et al., 1983). Viele (1989) divided the Ouachita Mountains into four tectonic provinces from north to south. They are 1) Ozark uplift-Arkoma basin, 2) Frontal thrust belt-Maumello zone, 3) Benton uplift-Broken bow uplift, and 4) Southern Ouachitas (Fig. 3). The Benton uplift contains thrust faults and folds with east-west trends during the late Paleozoic Ouachita orogeny (Babaei and Viele, 1992; Blythe et al., 1988). Seismic profiles around the Benton uplifts indicate both that main thrusts verge north and that the Ordovician to Mississippian strata in Benton uplift are allochthonous (Blythe et al., 1988). Richard et al. (2002) proposed that large-scale advective did not take place in Paleozoic strata in Ouachita orogeny, for formations have heterogeneous  $\delta^{18}\text{O}$  values and both vein and the adjacent host rock samples are similar in isotopic value.



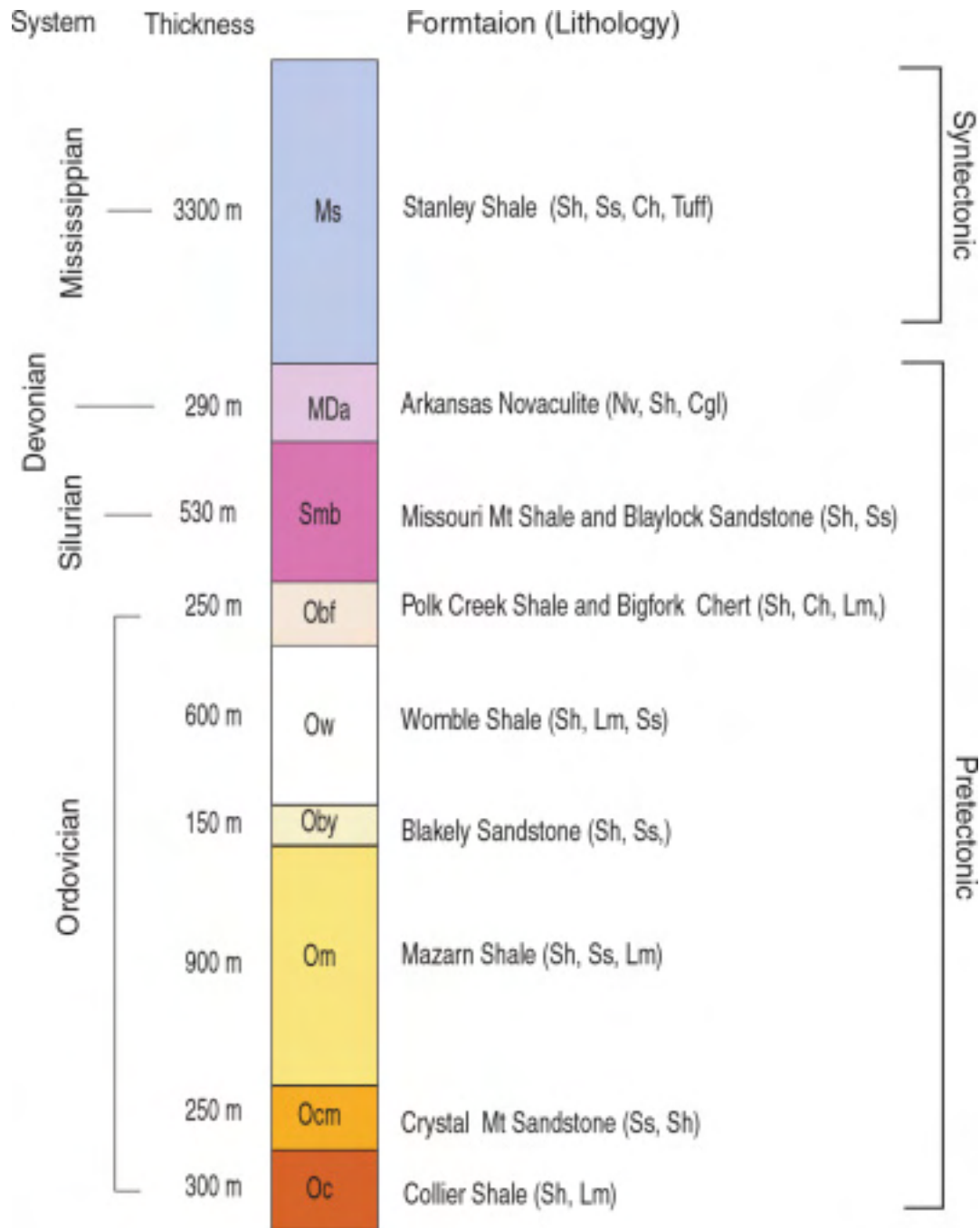


Fig. 2. Stratigraphic column in Paleozoic Ouachita Mountains in eastern Arkansas (after Howard and Stone, 1988). Sh: shale, Ss: Sandstone, Lm: limestone, Ch: chert, Cgl: conglomerate, and Nv: novaculite.

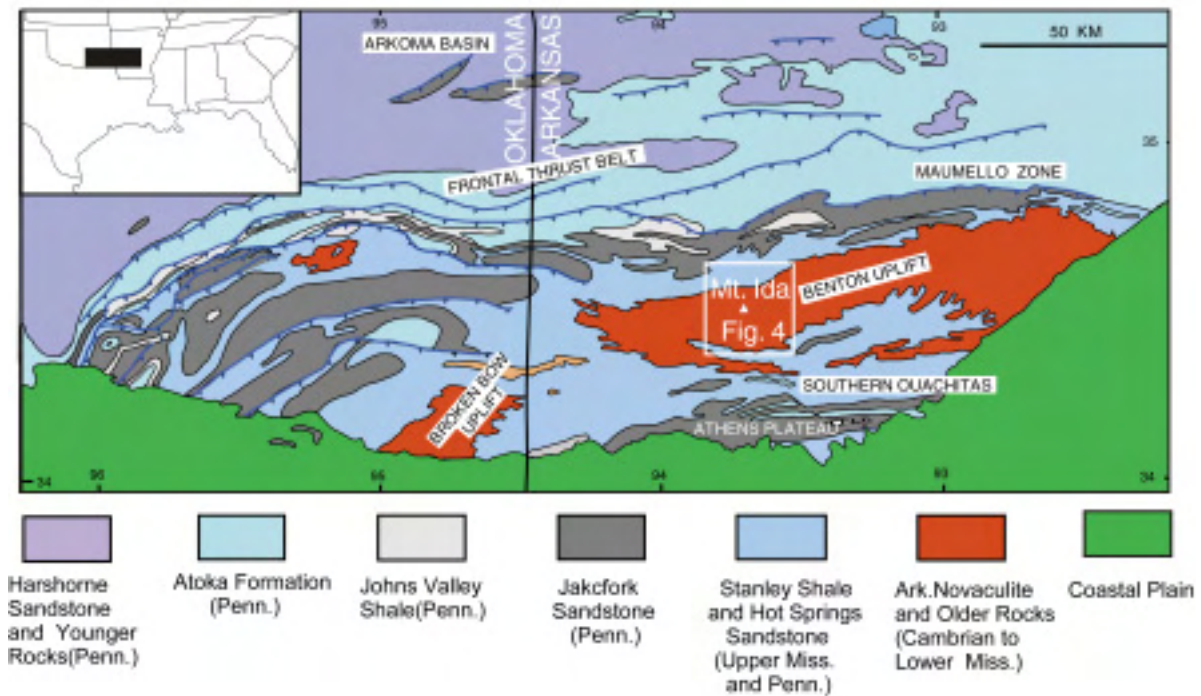


Fig. 3. Geological map of Ouachita Mountains (after Miser, 1959). Ouachita Mountains can be divided into four tectonic provinces from north to south: 1) Ozark uplift-Arkoma basin, 2) Frontal thrust belt-Maumello zone, 3) Benton uplift-Broken bow uplift, and 4) Southern Ouachitas.

Rock ages within the Benton Uplift range from Ordovician (Collier Shale) to Lower Mississippian (Arkansas Novacullite). The Upper Mississippian syntectonic Stanley Shale unconformably overlies the Arkansas Novaculite (Fig. 2). The Ordovician Womble Shale in Mountain Ida is exposed within north-verging thrusts and tight folds, some of which are locally isoclinal (Blythe et al., 1988; Haley and Stone, 1976; Pitt et al., 1961; Fig. 4). The Womble Shale consists mostly of black shale with thin layers of limestone, silty sandstone and some chert (Fig. 2; Howard and Stone, 1988). Milky quartz veins and cleavage are common in beds in the Womble Shale (Stone and Sterling, 1962; Howard and Stone, 1988). Minor amounts of fine to medium-grained frosted quartz grains, subgranular calcite and illite occur in the shale. The sandstone is fine to medium-grained. Variable amounts of quartz, feldspar, dolomite, and pyrite occur in the limestone. Black chert is found as thin layers within the upper portion of the Formation (MacFarland, 1998).

Figure 4b is a cross section constructed based on geological mapping (Haley and Stone, 1976) and previous interpretations (Blythe et al., 1988; Arbenz, 1984). Thrust sheets typically are south dipping and concave upward on the south flank of the Uplift. The fact that Womble Shale is surrounded by older formations such as Mazam Shale indicates the existence of a window in Benton Uplift. Uplift on a younger, deeper thrust fault ramp produced a broad anticline of overlying duplexed rocks (Miser, 1959; Lillie et al., 1983; Houseknecht and Matthews, 1985; Viele and Thomas, 1989). Miser (1959) proposed that the quartz veins mined for museum-quality crystals in the Ouachita Mountains formed late in the Uplift's history.

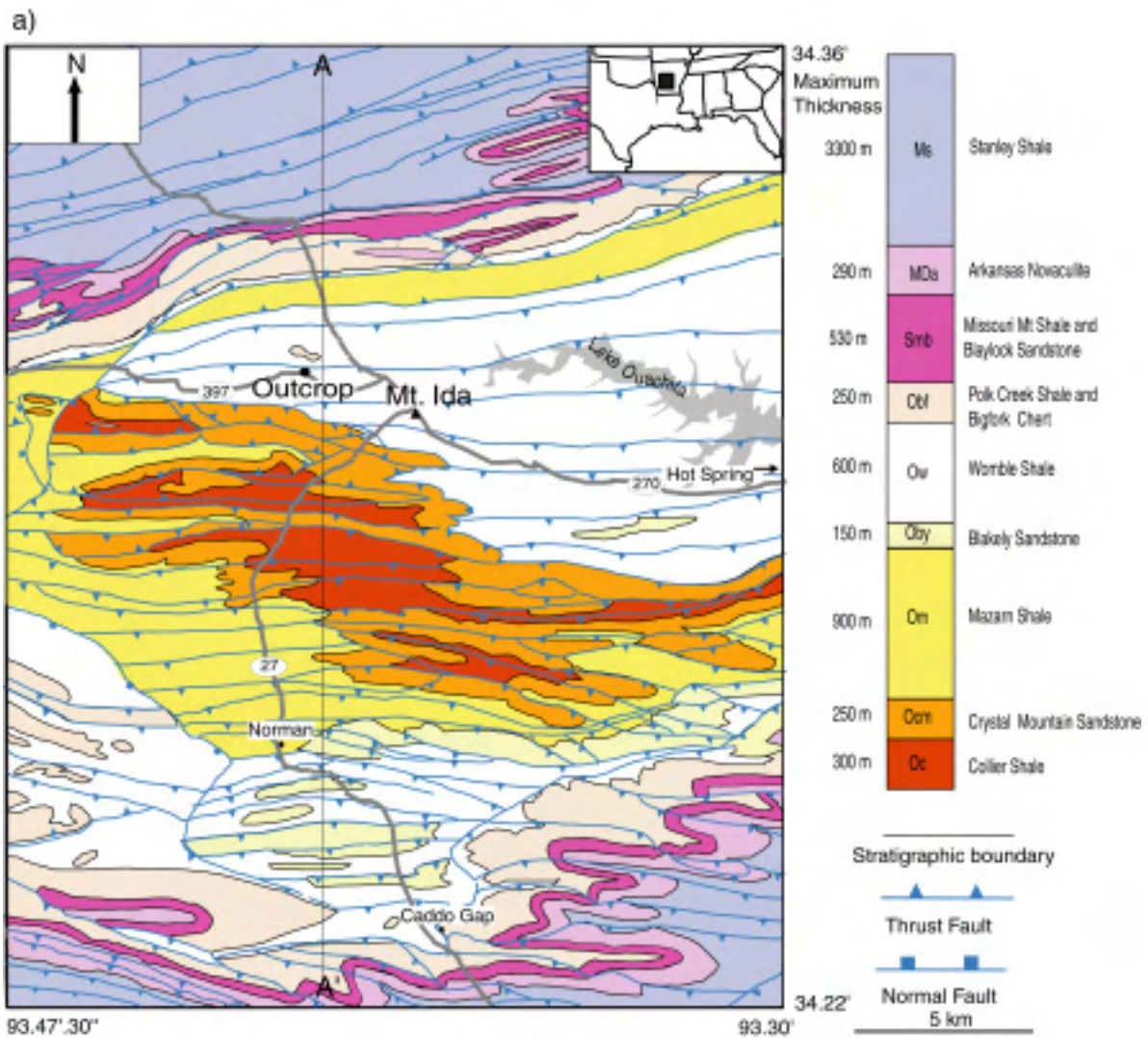


Fig. 4. a) Geologic map of study area around Mt. Ida in Arkansas (after Haley and Stone, 1976). b) Geological cross section along A-A' in Figure 5a. No vertical exaggeration. Formation symbols are same as Figure 4 a). c) Restoration of cross section along A-A'.

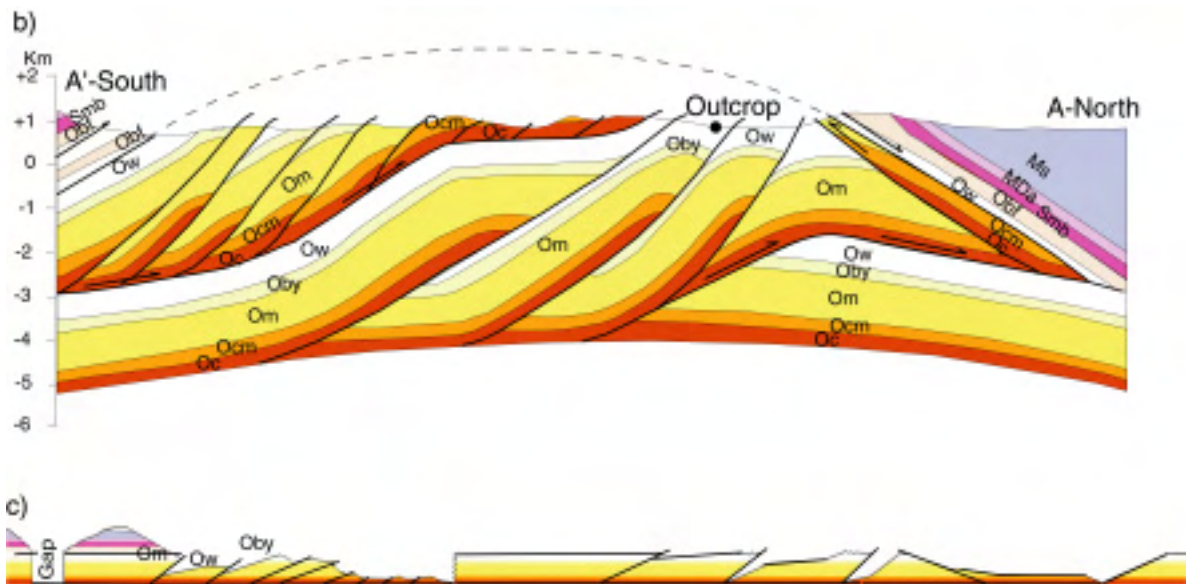


Fig. 4. Continued.

### 3. OUTCROP OBSERVATION

At our study site the Womble Shale is composed of alternating 3-20 cm thick shale beds and 3-30 cm thick calcareous sandstone beds (Fig. 5a). Most fibrous veins are normal to bedding.

Fibrous veins can be divided into 3 groups based on their host rocks (shale or calcareous sandstone) and vein orientations; 1) veins-in-shale (N68E), and 2) N45E veins, and 3) N7E veins (Fig. 5b-d, and Fig. 6).

Veins-in-shale are thin (1 ~ 5 mm) and show sharp vein-host boundaries. They are invariable finely fibrous. Not all shale layers contain veins.

N45E and N7E veins consist of calcite and quartz. N45E are 1-5 mm thick, which is typically thinner than the N7E veins (5-30 mm thick). N45E veins are fibrous and usually occur below shale layers; they may be contained in more coarse-grained beds. N7E vein fillings are more blocky and typically found in calcareous sandstone below calcareous sandstone layers containing N45E veins. Most veins don't cross lithologic boundaries. However, some of the N45E veins that cut calcareous sandstone are continuous with veins-in-shale (Fig. 6c). Joints are more easily seen in shale than calcareous sandstone beds. Joints in shale are parallel to both each other and veins-in-shale. Coarse, blocky, bed-parallel mixed quartz-calcite veins also occur in the outcrop. They appear to be later than all other veins.

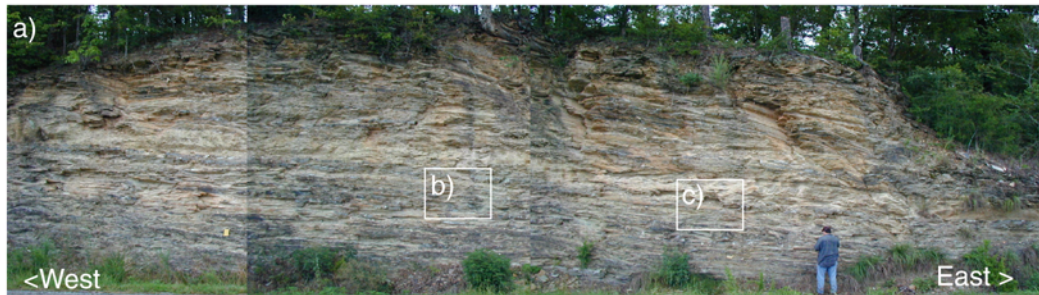


Fig. 5. a) Outcrop photograph of sample location in Womble Shale near Mt. Ida. b) N7E veins are typically found below the calcareous sandstone layers containing N45E veins, while N45E veins usually occur below shale. c) N45E veins layers are continuous with fibrous calcite veins-in-shale. Bedding-parallel quartz-calcite veins within calcareous sandstone. d) Simplified description of veins and their host rocks. Calcareous SS: calcareous sandstone, and Qtz-CC layer: quartz-calcite layer.



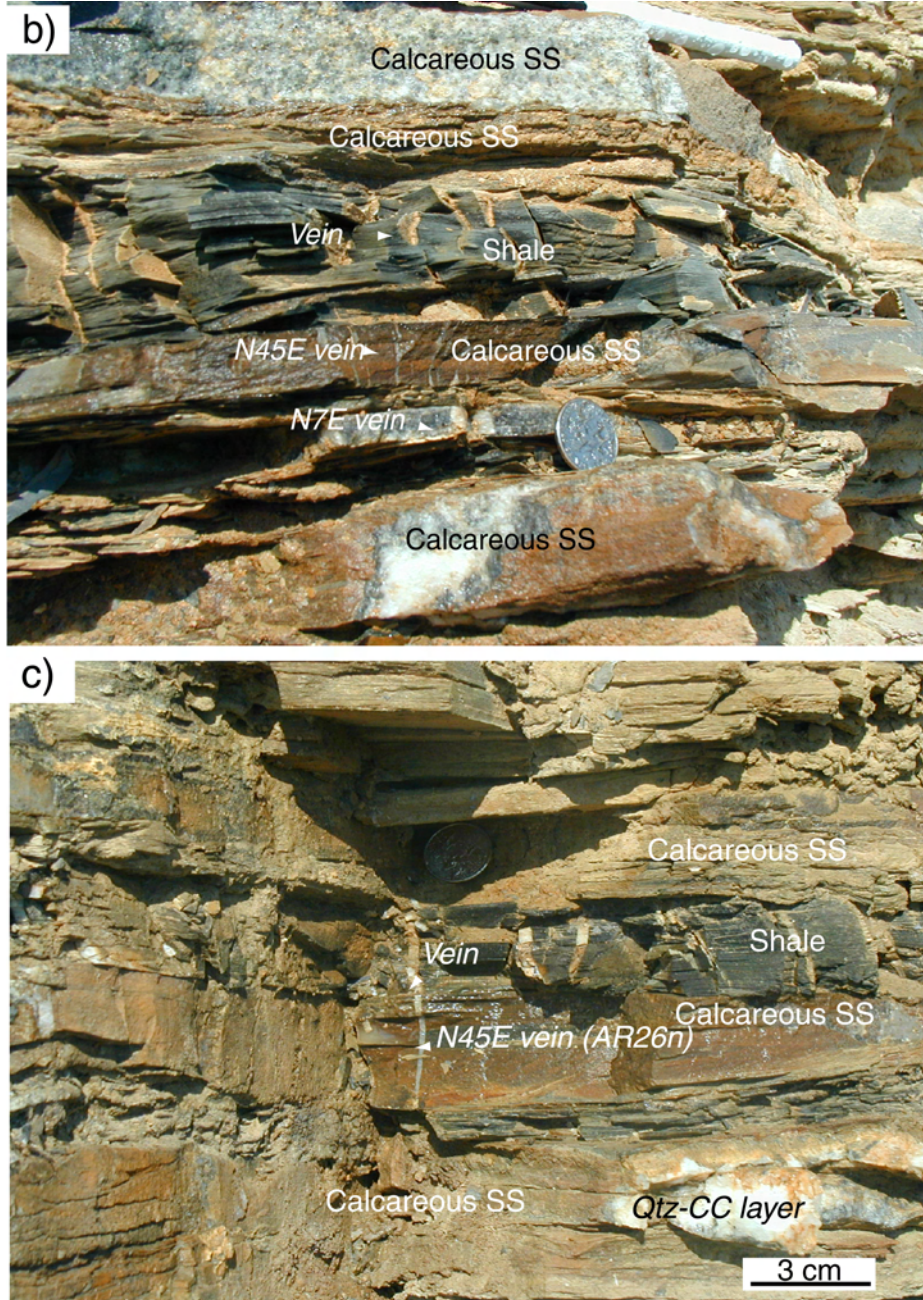


Fig. 5. Continued.



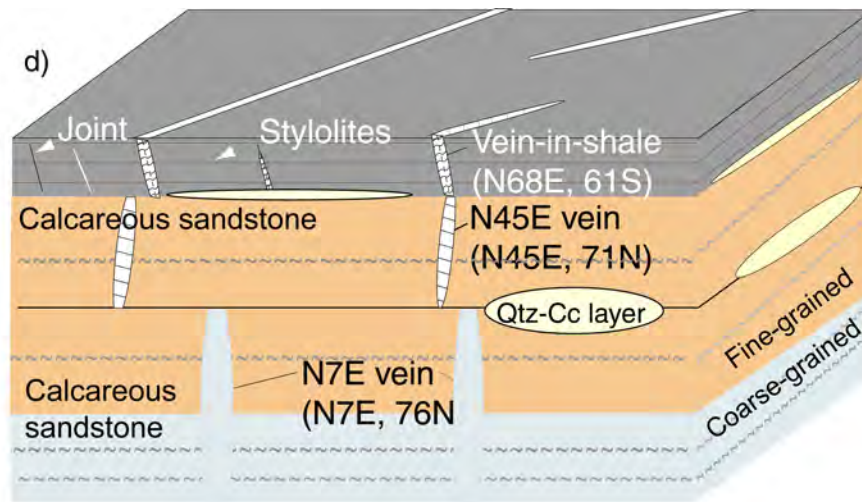


Fig. 5. Continued.

The transport direction in this area is south to north based on normals to both fold axes and regional thrust traces (Fig. 5a; Haley and Stone, 1976). More locally, the attitudes of beds in the outcrop (Fig. 6a) strike E-W and dip gently toward the north. The direction of N7E veins is parallel to the N-S presumed average tectonic stress direction (Fig. 6b). In contrast, N45E veins and veins-in-shale (N68E) trend oblique to the transport direction (Fig. 6c, d). In the field, the timing of veins cannot be established with certainty. However, veins-in-shale trend subparallel to N45E veins and rarely the continuity between the two indicate that veins-in-shale and the N45E veins form simultaneously.

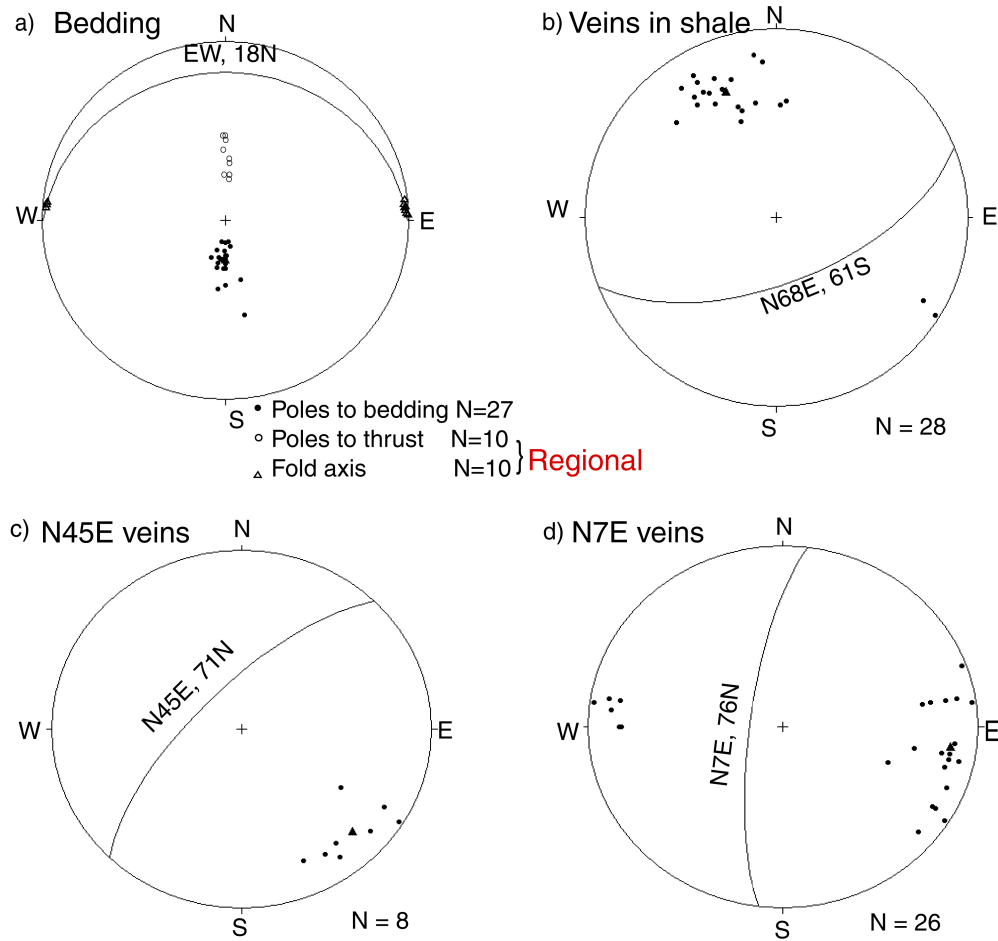


Fig. 6. Equal area, lower hemisphere projections of poles and average plane to a) bedding of shale and calcareous sandstone, and regional fold axes and normals to thrust faults, b) veins-in-shale, c) N45E veins, and d) N7E veins. Great circle shows average orientations of bedding and veins. N = number of poles.

#### 4. TEXTURES

Petrography and X-ray diffraction (XRD) reveal that the shale containing the veins-in-shale consists predominantly of mica and quartz. The calcareous sandstone containing the N45E veins is composed of fine-grained quartz, mica, and less calcite. The calcareous sandstone containing the N7E veins contain calcite-poor and calcite-rich fractions. The calcite-poor beds are composed of fine-grained of mica, quartz, and less calcite. The calcite-rich layers are composed of coarser-grained quartz, calcite, and less mica (Fig. 7h). Vein fibers of the N7E veins are mostly composed of calcite fibers where the vein is hosted in the calcite-poor beds. Stylolites are present in all lithologies in the outcrop, although more easily distinguished in shale. Description of veins and their host rocks is summarized in Table 1.

Vein grains in shale are mostly fibrous calcite that have widths ranging from 150 to 200  $\mu\text{m}$ . There is no evidence of recrystallization. Calcite fiber boundaries are not serrated and the fibers are perpendicular to the median line, curving moderately ( $0^\circ$  to  $25^\circ$ ) towards the vein wall (Fig. 7a). Veins-in-shale commonly display a quartz rim or 'quartz selvage' in the usage of Hilgers and Urai (2001) at the vein wall (Fig. 7a-b). The vein's center commonly displays a median line of mica inclusions, but inclusion bands or trails are not observed elsewhere (Fig. 7a-c). As described before, these veins consist of different material from wall rock. This feature is similar to 'antitaxial' veins proposed by Ramsay and Huber (1983).

Also, the vein, which is normal to stylolites, is cut by well-developed stylolites that are spaced apart from 0.5 mm to 1 mm (Fig. 7d). Stylolites are predominantly bedding-parallel and they are continuous through vein arrays.

Table 1. Description of veins and their host rocks.

---

|   |
|---|
| Fibrous calcite vein (1-5 mm thick)                           |
| Host rock – Shale   |
| N45E vein (1-5 mm thick)                                      |
| Host rock - Calcareous sandstone (quartz, mica, less calcite) |
| N7E vein (5-30 mm thick)                                      |
| Host rock - Calcareous sandstone                              |
| Calcite-poor layer (quartz, mica, less calcite)               |
| Calcite-rich layer (quartz, calcite, less mica)               |

---

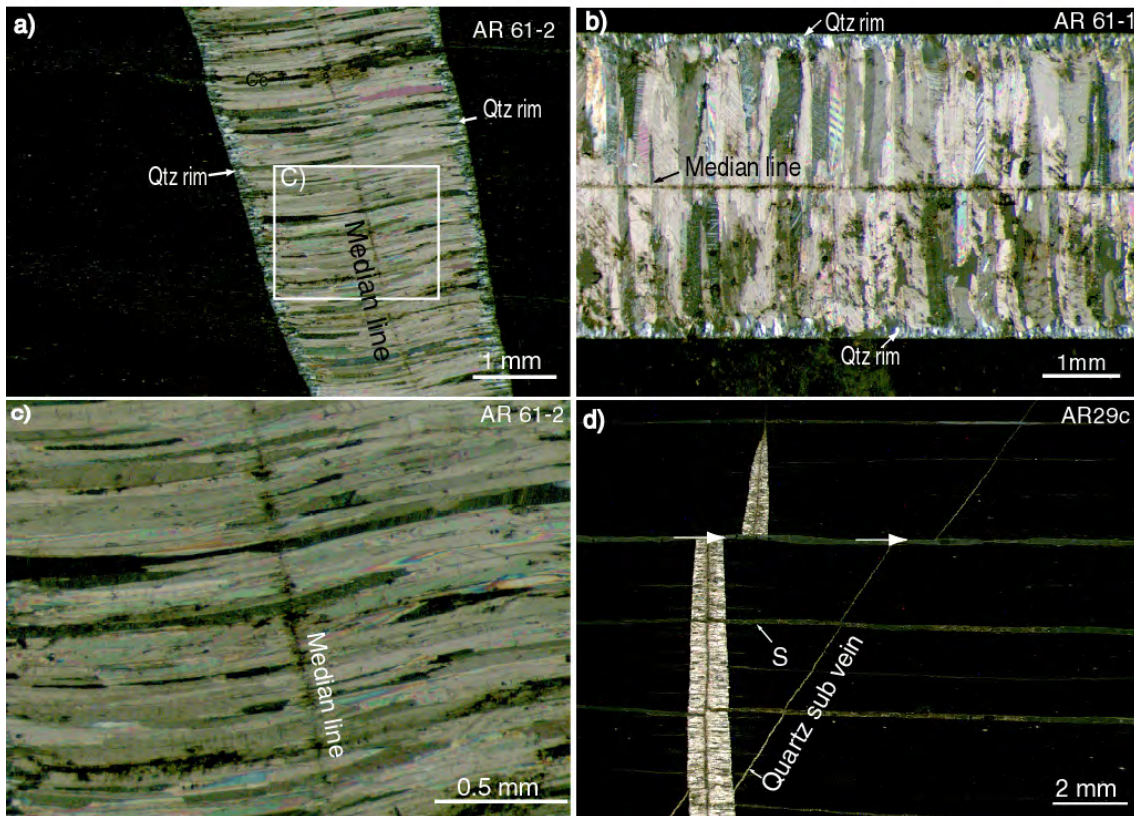


Fig. 7. Photomicrographs of thin sections. a)-d) veins-in-shale. e)-f) N45E veins. g)-h) N7E veins. For veins-in-shale, quartz rim is found between vein and wall rock: a) bedding normal view, b) bedding parallel view. a) Fibers are perpendicular to the median line and slightly curved towards the vein wall. c) Vein likely grows along vein-wall boundary rather than median line due to the fact that most of vein grains are continuous across the median line. d) Vein cross-cutting relationship between main vein and subvein and vein cutting by shear movement along stylolites. e) Length/width ratio of vein crystals. The Length/width ratio increases from the coarse-grained layer toward the fine-grained layer. f) Saw-tooth (serrated) texture is shown in grain boundaries. g) N7E veins consist of fibrous or blocky calcite near the vein wall and blocky quartz grains in center which are wider than calcite grains. h) Calcareous sandstone containing N7E veins is grouped into two layers: fine grained calcite-poor layer (CPL) and coarse-grained calcite-rich layer (CRL). Cc: calcite, Qtz: quartz, S: stylolites, and St: saw-tooth (serrated) texture.



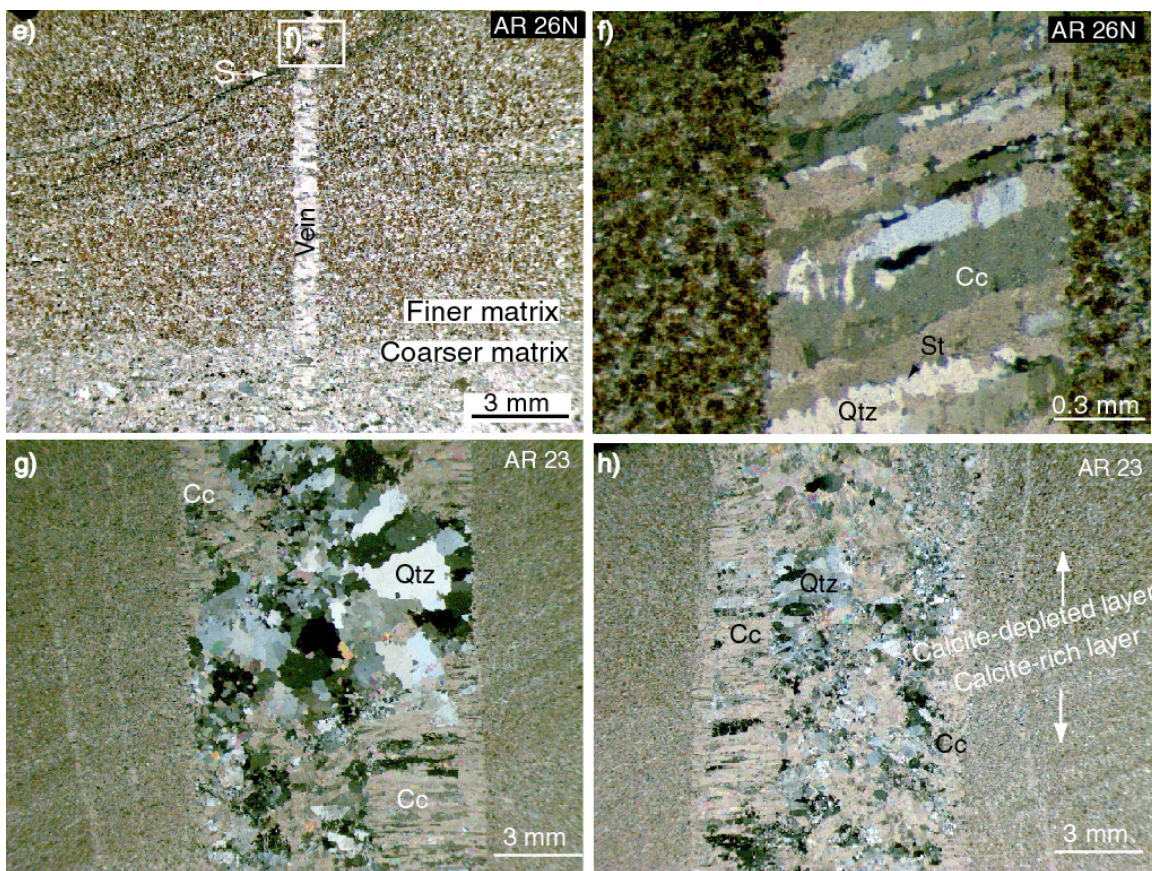


Fig. 7. Continued.

N45E veins are mostly composed of fibrous calcite and quartz with fiber widths ranging from 300 to 500  $\mu\text{m}$ . The length to width ratio of grains in the vein increases as the host grain size decreases. Vein grain size also is roughly proportional to the host grain size (Fig. 7e). N45E veins can be further characterized by 1) indistinct vein-wall boundaries, 2) minerals represented in the host, 3) no median line of inclusion bands. In addition, thinner individual veins of this orientation show serrated grain boundaries. This fabric is similar to 'stretched' fibrous veins described by Ramsay and Huber (1983).

N7E veins consist of fibrous calcite at the vein-wall boundary, and blocky quartz and calcite grains in the center. N7E veins mostly show the same characteristics as N45E veins (Fig. 7g-h). Vein grains are not continuous from the vein-wall to the opposite side (Fig. 7g-h). As with N45E veins, grain size seems to be roughly proportional to the grain size of the host. Several thinner (50 to 100  $\mu\text{m}$ ) microveins are parallel to the main veins (see Fig. 8a). Inclusion trails are found in vein grains, but they are not continuous to adjacent grains (see Fig. 8f-h).

## 5. RELATION BETWEEN MATRIX GRAIN SIZE AND VEIN FIBERS

N7E vein (AR30) were analyzed to determine the relationship between host grain size and the size of vein fibers. In thin section, both the fibrous and blocky calcite grains in N7E veins are present along the vein (Fig. 8a). The relationship of the matrix-surrounding vein vs. the length-to-width ratio of vein fibers was quantified by surveying the size of grains along the vein in sample AR30. The lengths and widths of vein grains were measured parallel and normal to long axes of the vein fibers (Fig. 8a, b).

The host can be divided into two layers based on calcite grain size. These are coarse-grained ( $>0.02 \text{ mm}^2$ ) and fine-grained ( $<0.01 \text{ mm}^2$ ) layers. In both, equant quartz grains roughly proportional to host grain size occur within the vein. They are randomly distributed and don't contact vein-wall (Fig. 8e and h). Small equant quartz grains of  $10 \mu\text{m}$  width are present between the vein and host in the fine-grained layer (Fig. 8f). Vein-wall boundaries are unclear (Fig. 8c-e) in the coarse-grained layer, while vein-host boundaries are relatively more distinguishable in the fine-grained layer. About 70 % of fiber grain boundaries of calcite are located at the peaks of ethereal host grains.



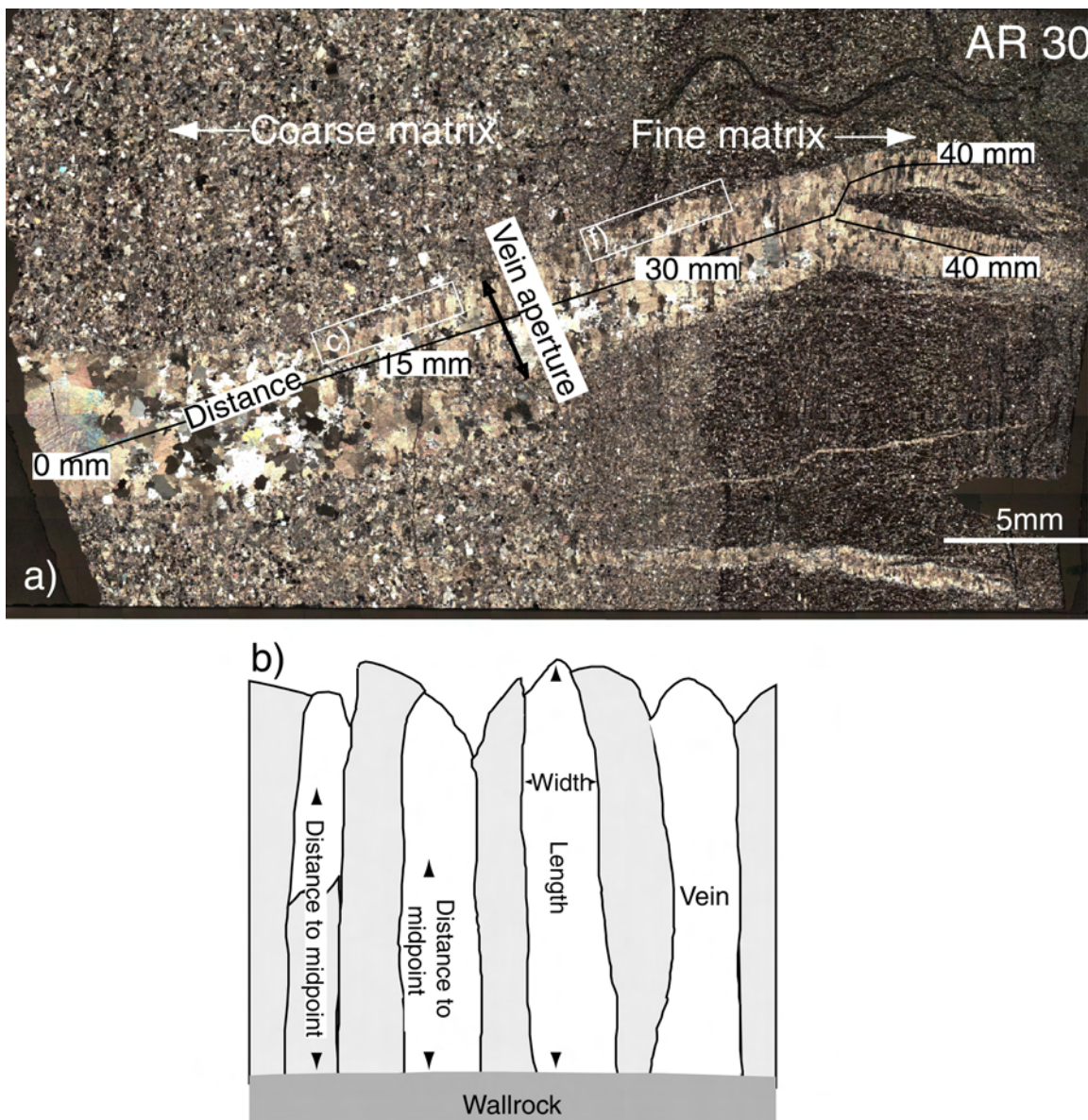
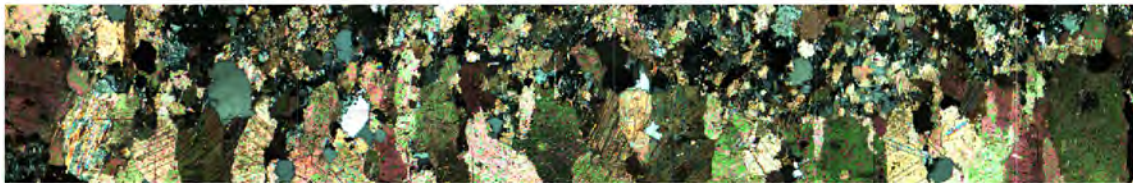


Fig. 8. a) Photomicrograph of thin section (AR30) showing the relationship between the matrix and N7E vein fibers. Numbers refer to the distance from an arbitrary origin on the left used to make the measurements in Fig. 9. b) Length and width of vein grains were measured parallel and normal to long axes of the grains. c-h) Photomicrographs of vein-wall boundaries and sketches in coarse matrix layer (c-e) and fine matrix layer (f-h).



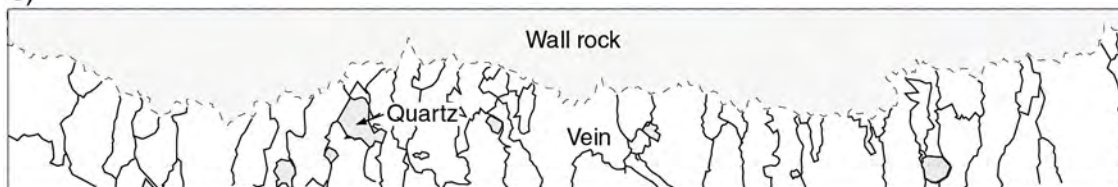
c) Coarse matrix Crossed nicols



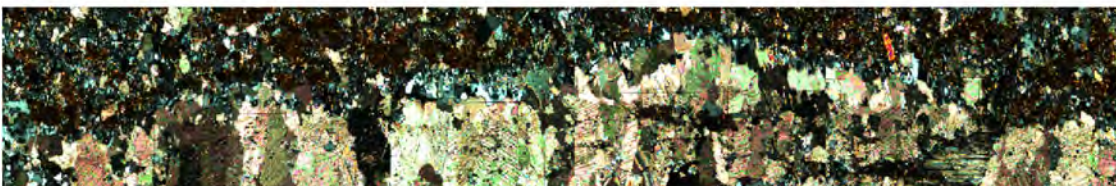
d) Plane light



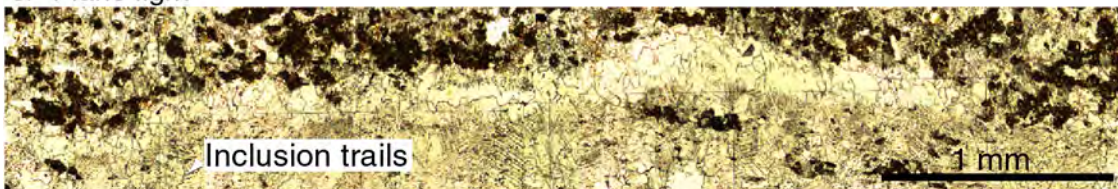
e)



f) Fine matrix Crossed nicols



g) Plane light



h)

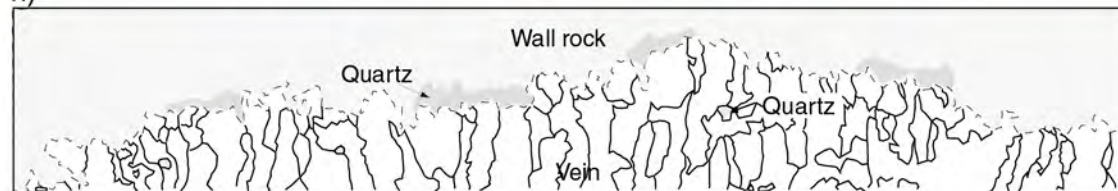


Fig. 8. Continued.

The host grain size decreases with distance along the vein (Fig. 9a). Figure 9a shows that within the coarse-grained layer the length-to-width ratio is proportional to decreasing matrix size. By contrast, there is no strong relationship between length-to-width ratio and matrix size reduction in the fine-grained layer region; both fibrous and equant vein grains are found in the fine-grained host layer. Vein fiber width also decreases with decreasing matrix size (Fig. 9b), i.e., less than 0.04 mm in the fine-grained layer and 0.01-0.07mm in the coarse-grained layer.

Vein fiber lengths do not show any particular trend in relation to distance along the vein or host grain size (Fig. 9c). Instead, fiber length simply tracks the width of the vein.

Quartz grain size within the host decreases with distance along the vein through the transition from the coarse- to fine-grained host layers. Fig. 9d shows that vein quartz grains are mostly blocky with low length-to-width ratio, and show no relationship to host grain-size.

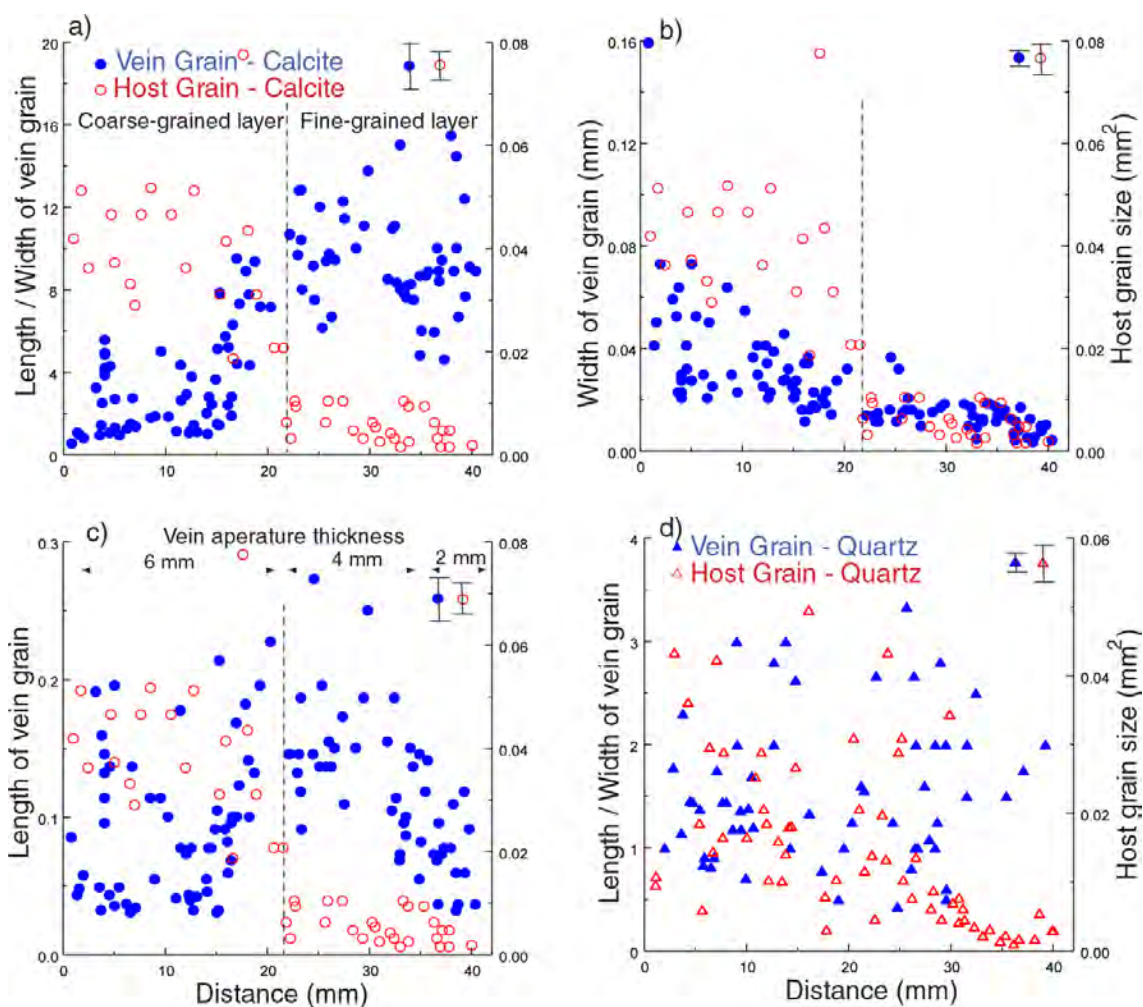


Fig. 9. Size and shape relationships of N7E vein calcite (a-c), quartz (d) and matrix in calcareous sandstone sample AR30. All are measured versus distance along the vein . a) The length / width (L/W) ratio of vein grains versus host grain size. b) Fiber width versus host grain size. c) Vein fiber length versus vein width. In the fine matrix, the length of vein fibers is proportional to vein aperture thickness. d) Vein quartz L/W versus the matrix grain size. Quartz grains consisting of vein are mostly blocky with low L/W ratio, showing no relationship to matrix size.

## 6. CHEMICAL COMPOSITION AND ZONING

Microprobe mapping was used to determine the chemical composition of both the vein and host. If both dissolution of wall rock and precipitation in veins are transport limited, chemical concentration gradients of vein-filling mineral may exist between the wall rock and the vein. In addition, cathodoluminescence (CL) was used to determine chemical zonation in the veins.

### *6.1. Methods*

A Cameca SX50 Electron was used to chemically analyze the area around veins over areas of  $512 \times 512$  pixels,  $30 \mu\text{m}$  (for  $15 \text{ mm} \times 15 \text{ mm}$ ) and  $2 \mu\text{m}$  (for  $1 \text{ mm} \times 1 \text{ mm}$ ) grid spacing per pixel. The beam conditions used were  $1 \mu$  diameter beam at 15 kV and 20 nA.

### *6.2. Veins-in-shale*

X-Ray diffraction (XRD) and the distribution of Si + Al + K both indicate that mica and quartz are the dominant minerals within the shale. Quartz is present on both the rim and tip of the vein (Fig. 10, Fig. 11, and Fig. 12). The presence of quartz in the vein tip indicates that quartz predated calcite precipitation in these veins.



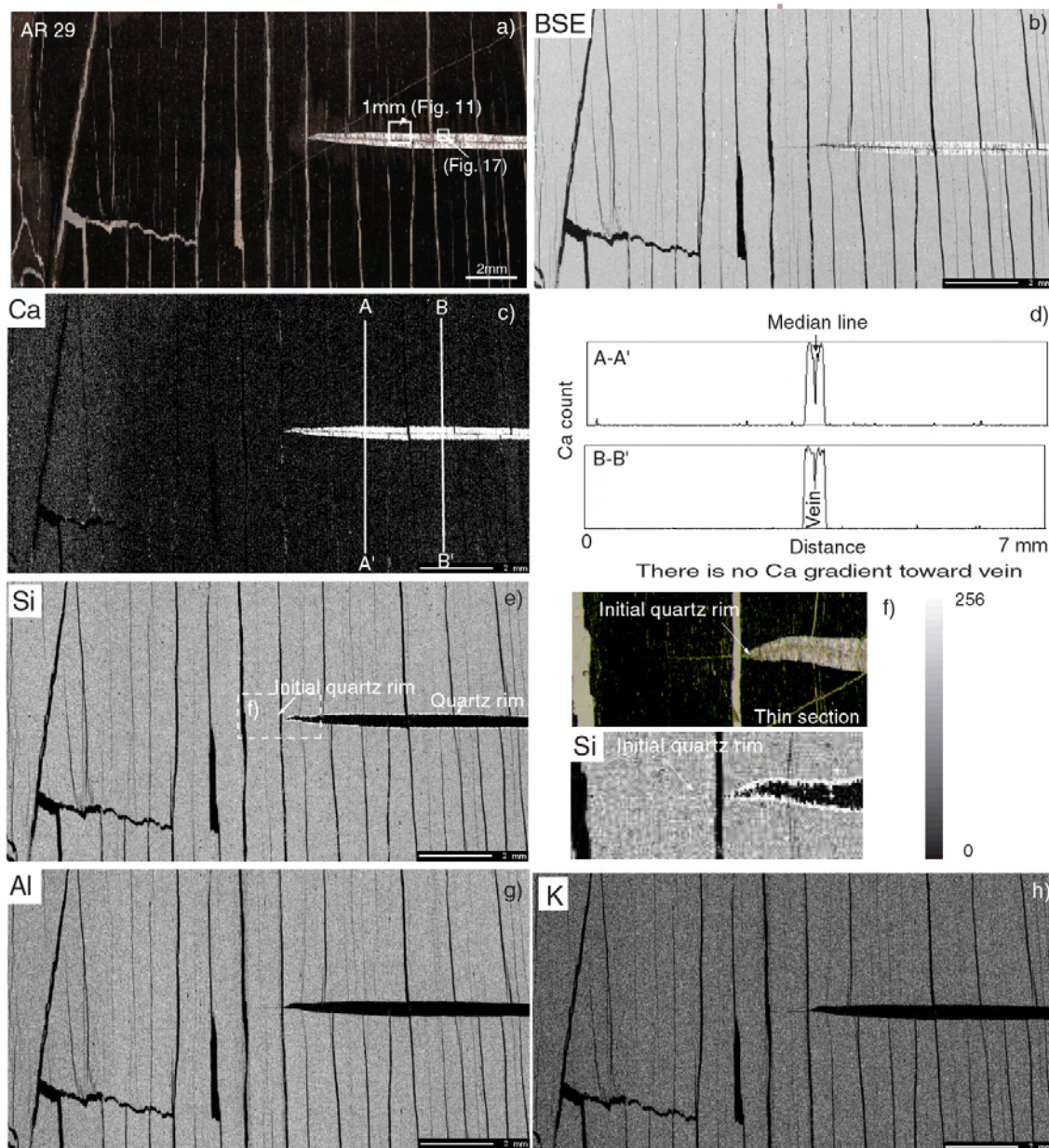


Fig. 10. Chemical composition map of vein and host rock of shale (AR29). a) Detailed microprobe map (1mm × 1mm) and cathodoluminescence are shown in Figure 11 and Figure 17, respectively. b) Back-Scatter Electron (BSE) image. c) Calcium map. Calcium concentration is low in shale. d) Profiles (A-A' and B-B') of calcium across vein. There is no Ca gradient toward the vein. e) Si map. Quartz is present in the vein-wall boundary and the tip of the calcite vein. f) Enlarged view of vein tip area. The quartz presence in vein tip without vein calcite indicates that quartz predated calcite precipitation in vein. g)-h) Al and K distributions. The shale consists of mica and/or K-feldspar.

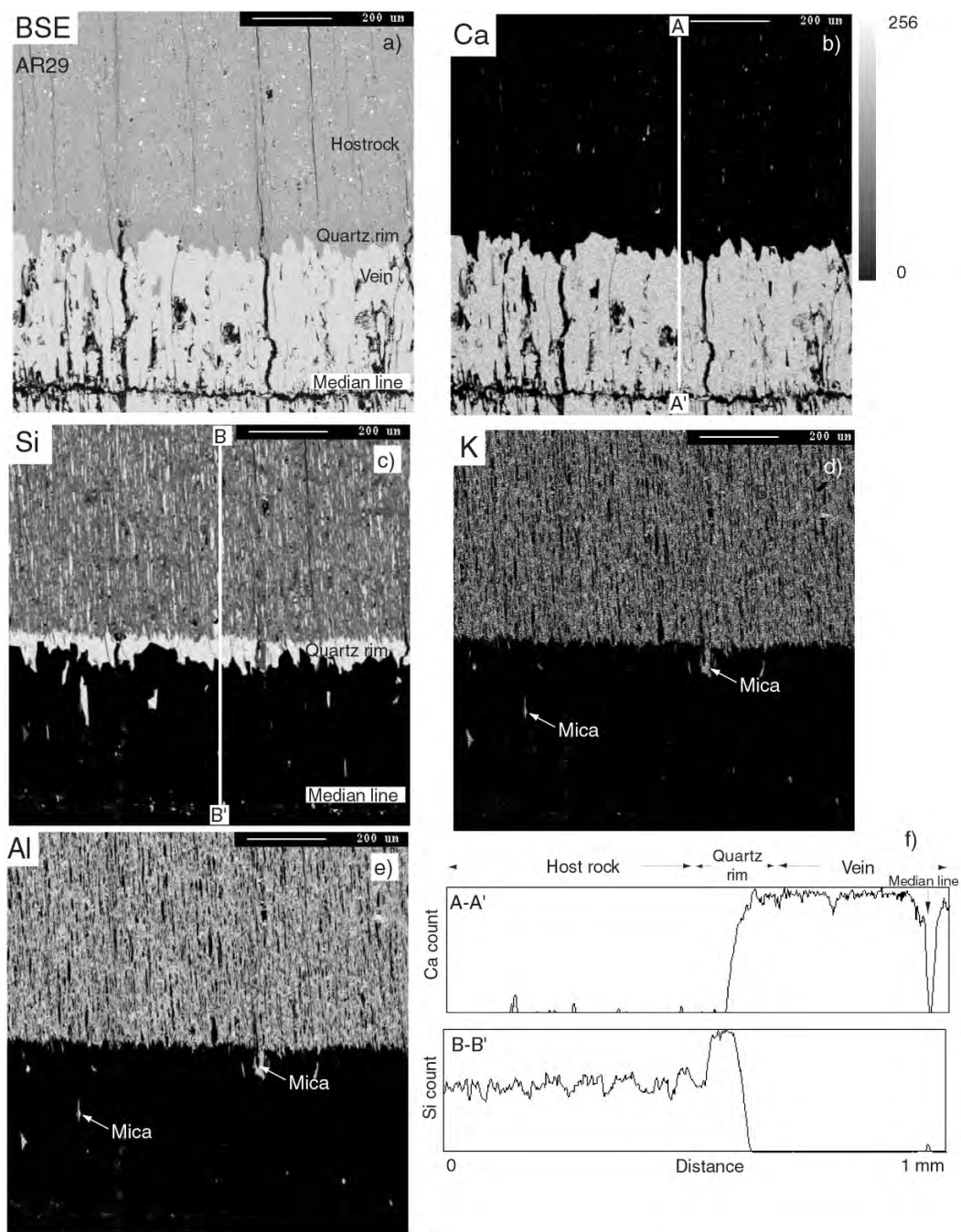


Fig. 11. Chemical composition map of vein and shale host rock (AR29). (a) Back-Scatter Electron (BSE) image. (b) Ca element map. (c) Si element map. The distribution of Si in the vein-wall boundary shows that quartz is present in the rim. (d) K element map. (e) Al element map. Si, K and Al distributions show that small grains of mica are irregularly present both within the quartz rim and the vein. (f) Profiles of Ca and Si, locations in (b) and (c), respectively. No gradient in either Ca or Si is apparent from the host toward the vein.

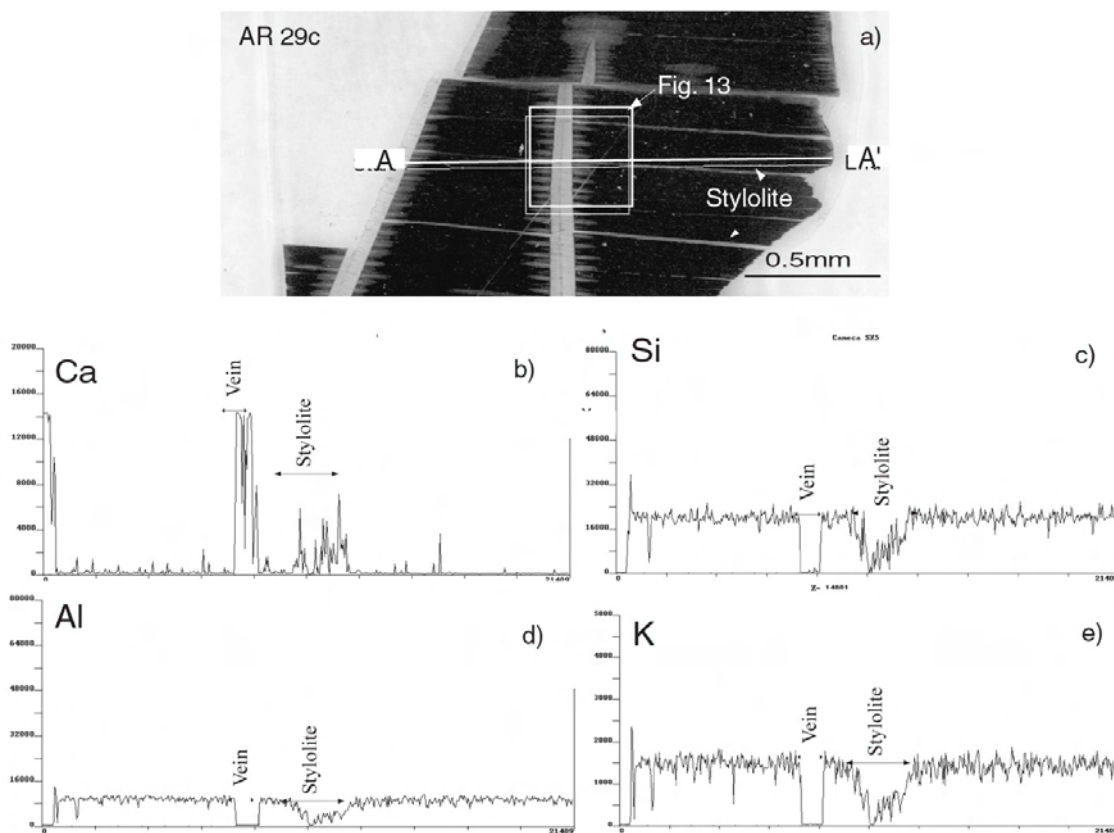


Fig. 12. Chemical profiles of vein, stylolites, and shale (AR29c). a) Thin section viewed on bedding. b) – e) element profiles along A-A' in a) of Ca, Si, Al and K, respectively. a) Ca is more enriched in the stylolite than in the shale, while Si, Al, and K are more depleted in the stylolite.



The distribution of Si + Al + K shows that small grains of mica are present both within the quartz rim and the vein (Fig. 11). Regularly orientated inclusion bands and trails are absent in the veins-in-shale samples. Small quartz grains are randomly present within veins and as well as being organized along the vein median line (Fig. 11).

Ca is not present in the matrix (Fig. 10, Fig. 11, and Fig. 12). The profiles of Ca across host rock and veins show that there is no Ca gradient between the veins and wall rock (Fig. 11 and Fig. 12). Stylolites consist of calcite + quartz + illite (Fig. 13b). Na, Mg, Fe, and Mn are below the detection limit in both the vein and shale.

Due to the lack of both Ca in the host and gradients of any sort in other elements, I conclude that either the vein calcite was derived from elsewhere or the entire rock has been highly altered after vein formation. The latter scenario can be ruled out, because recrystallization textures within the calcite veins was not found.

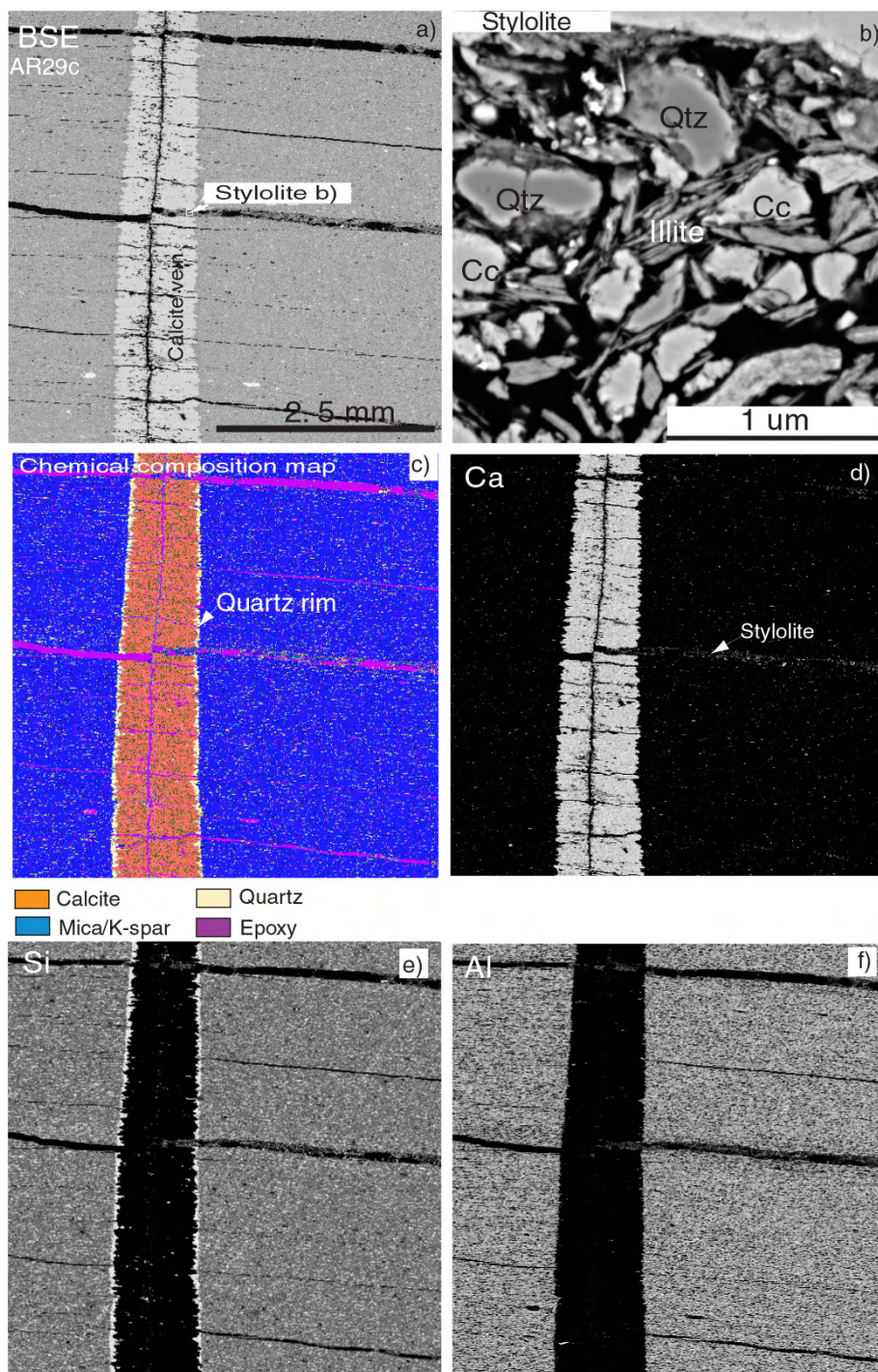


Fig. 13. Chemical composition map of vein-in- shale host rock of sample AR 29c. a) Back-Scatter Electron (BSE) image. b) Enlarged view of stylolites in Figure 13a reveals that stylolites consist of calcite, illite, and quartz. c) Composite map was created using 8 additive X-ray maps of Ca, Si, Al, K, Na, Mg, Fe, and Mn. shown in d)-k), respectively, Note in d) that Ca is more abundant in the stylolite.

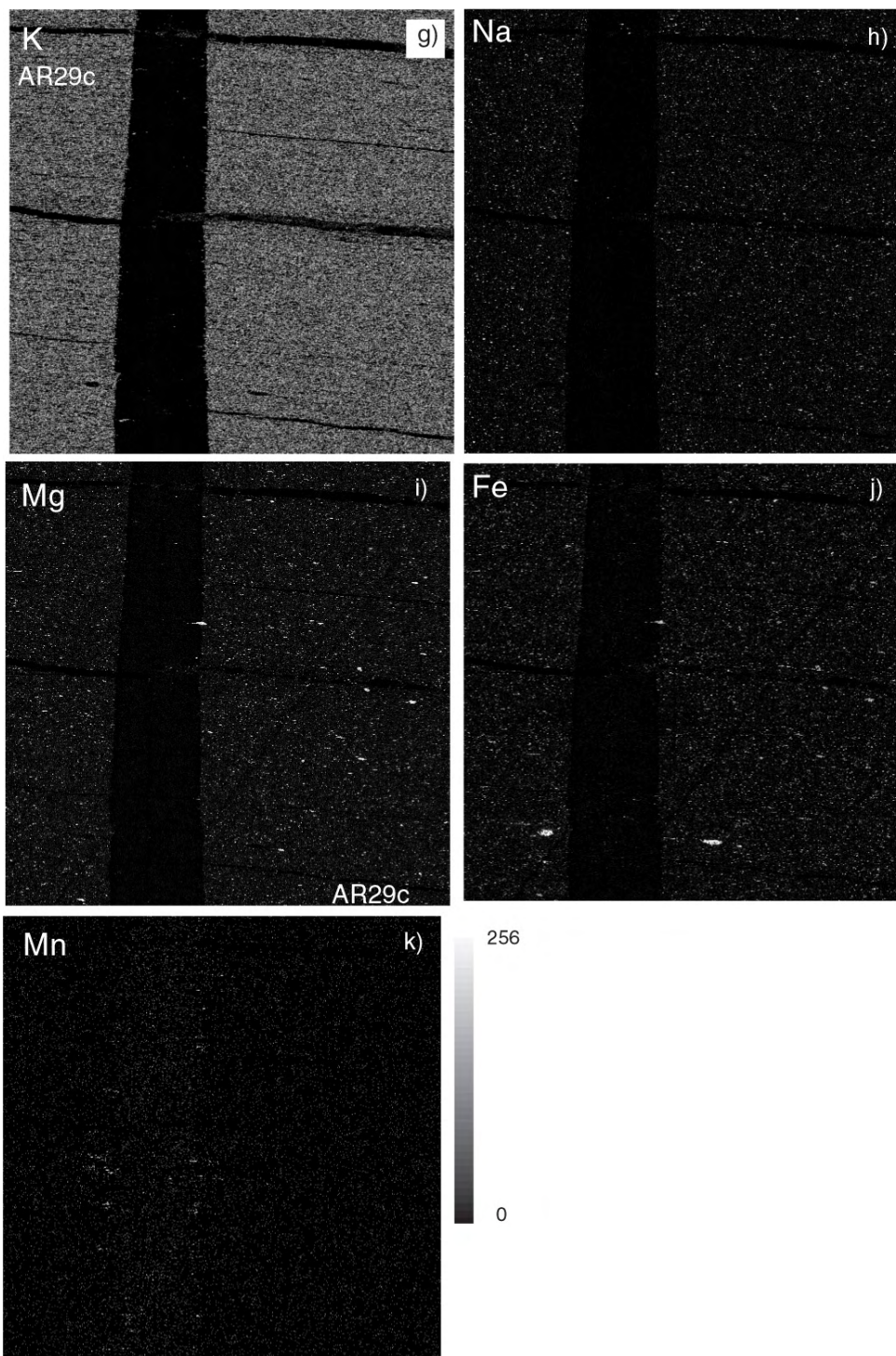


Fig. 13. Continued.

### 6.3. N7E vein

X-Ray diffraction (XRD) analysis and the distribution of Ca ± Si ± Al ± K reveals that mica, quartz, calcite, K-feldspar, and albite are the main minerals within the host. The vein consists of mostly calcite and randomly distributed quartz grains (Fig. 14a, and Fig. 16a). Ca concentration profiles across the host and vein show that there is no measurable gradient in the vicinity of the veins (A-A', B-B', and C-C', Fig. 14b-d). Stylolites within the host are composed of mica. Calcium is depleted in stylolites, suggesting that calcite is removed from stylolites. No gradient in Ca in the wall rock adjacent to veins indicated by microprobe confirms what is clear optically, namely, that the Ca is more abundant in calcite-rich bed with the coarse matrix than calcite-poor bed with fine matrix (Fig. 15).



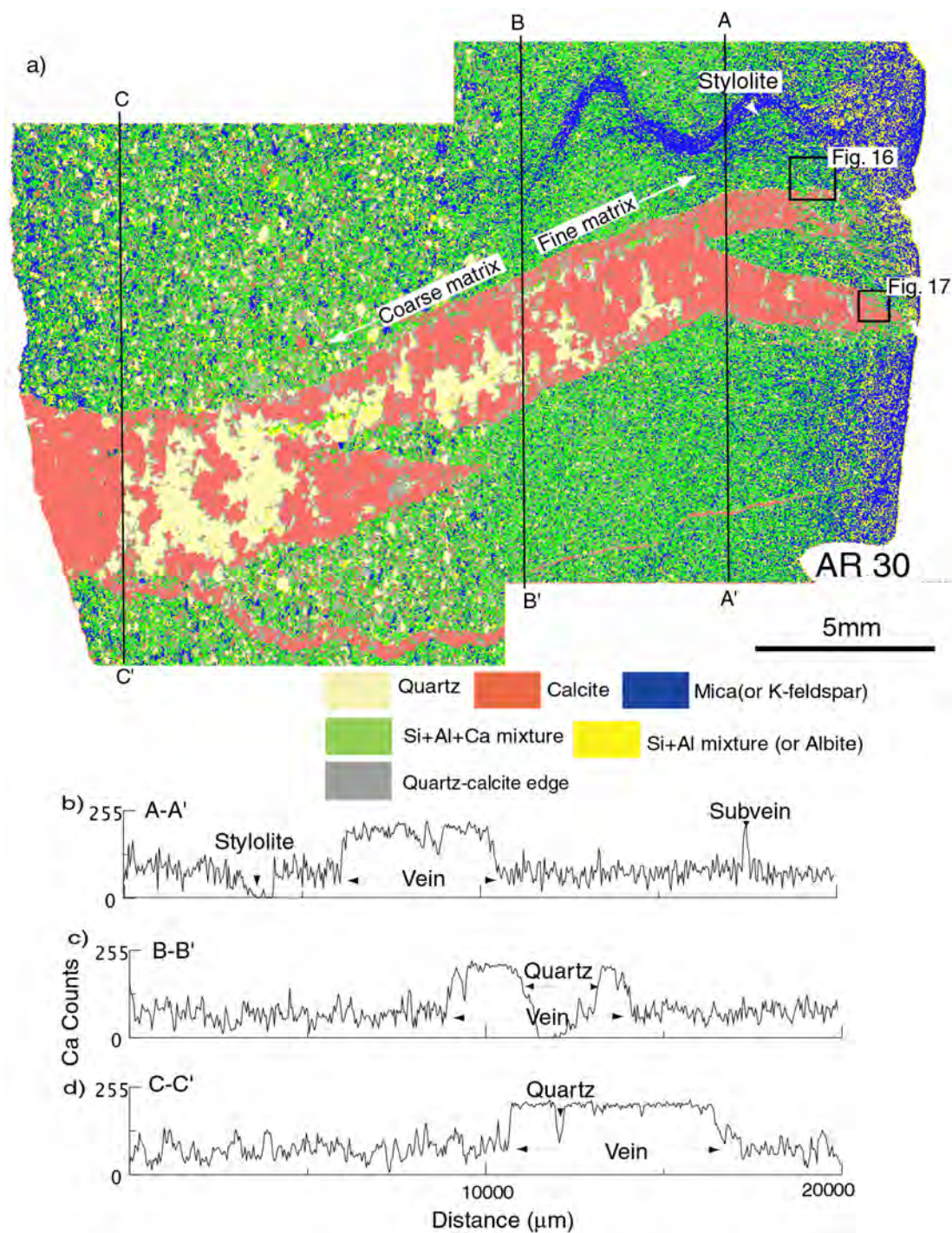


Fig. 14. a) Compositional map of N7E vein (AR30). The map was created using 4 additive microprobe maps for Ca, Si, Al, and K. b)-d), profiles of counts for Ca along profiles A-A, B-B', and C-C', respectively; profiles are located on a). There is no significant Ca gradient toward vein. A-A' profile reveals that Calcium is more depleted in stylolites.

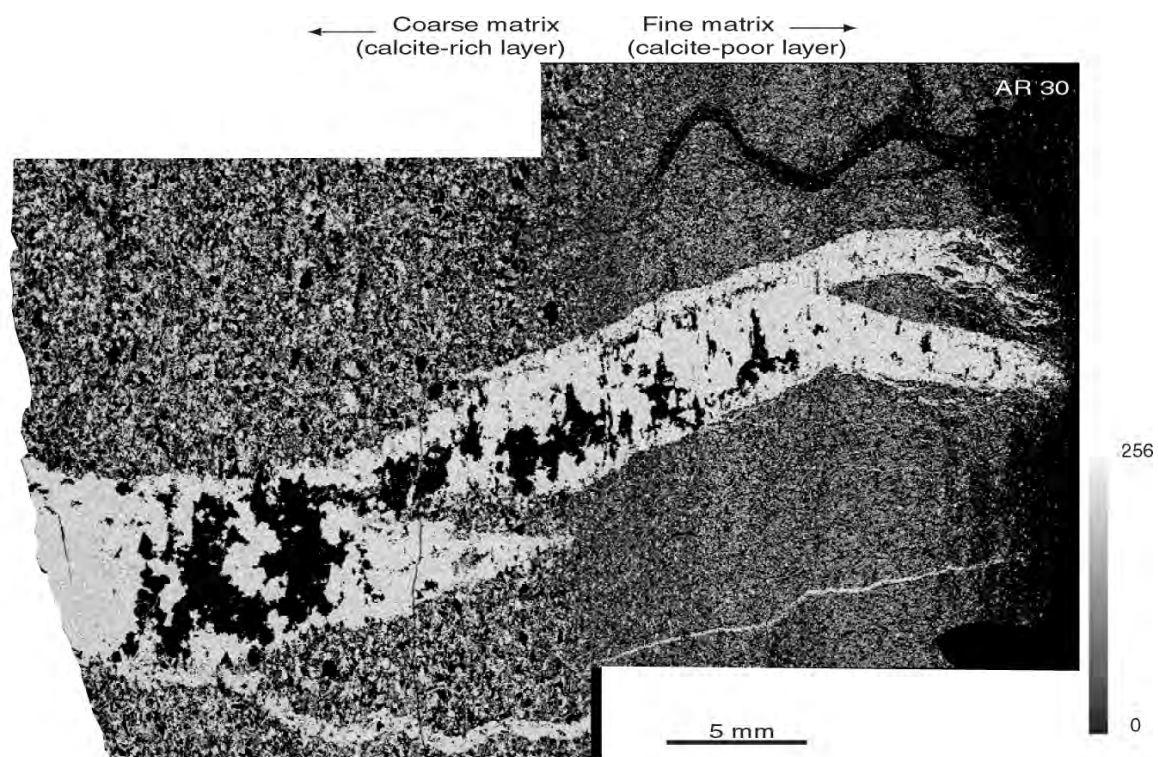


Fig. 15. Ca count in N7E veins and matrix from Figure 14 (AR 30) shows that the Ca is more abundant in coarse matrix (CRL) than fine matrix (CPL).



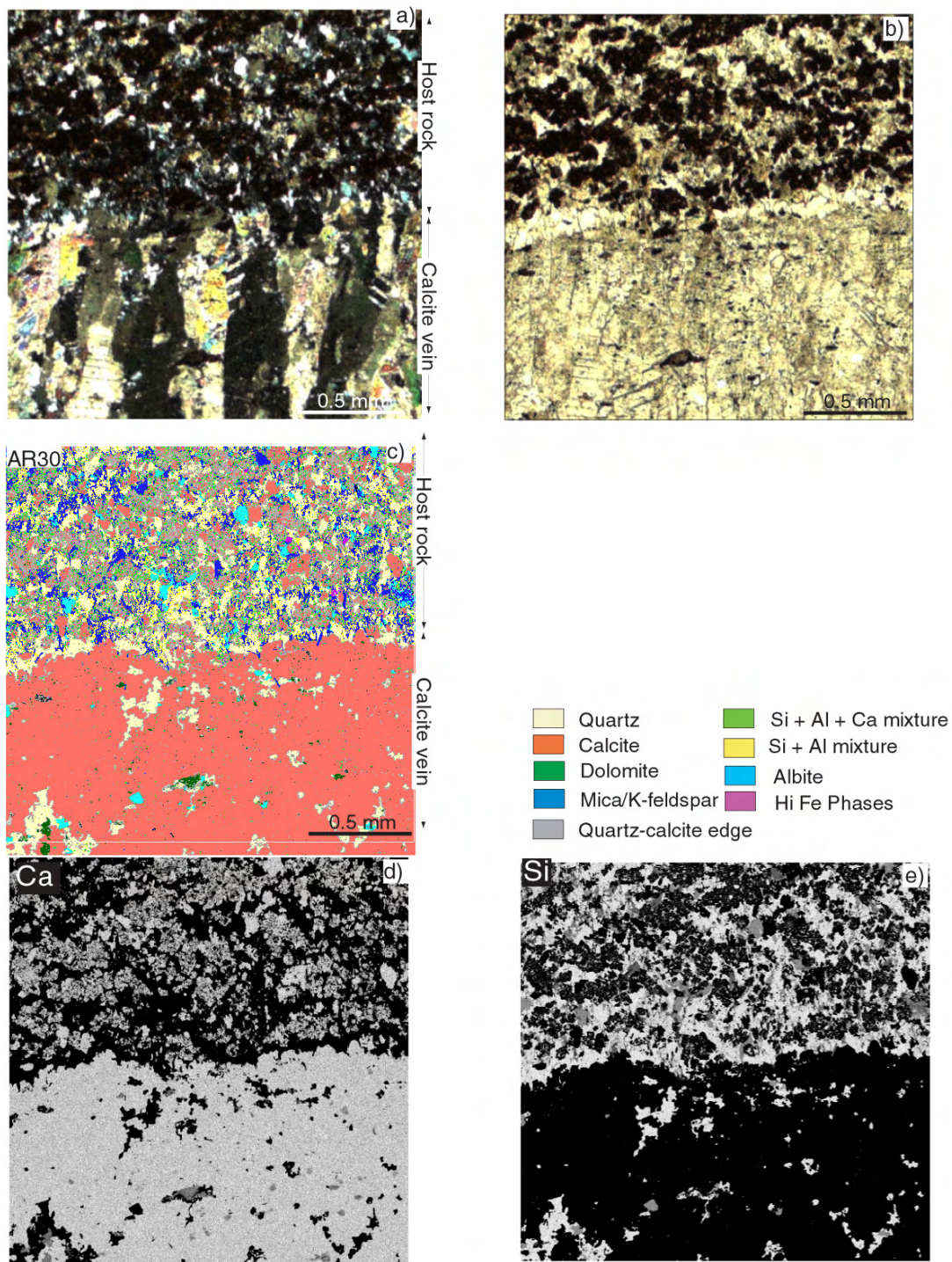


Fig. 16. Enlarged photomicrographs (a: cross nicols and b: open nicol), and microprobe maps of N7E vein and calcareous sandstone, located on Figure 14. Composite map (c) was created using 8 adding together X-ray maps of Ca, Si, Al, K, Fe, Mg, Mn, and Na shown in d)- l), respectively.

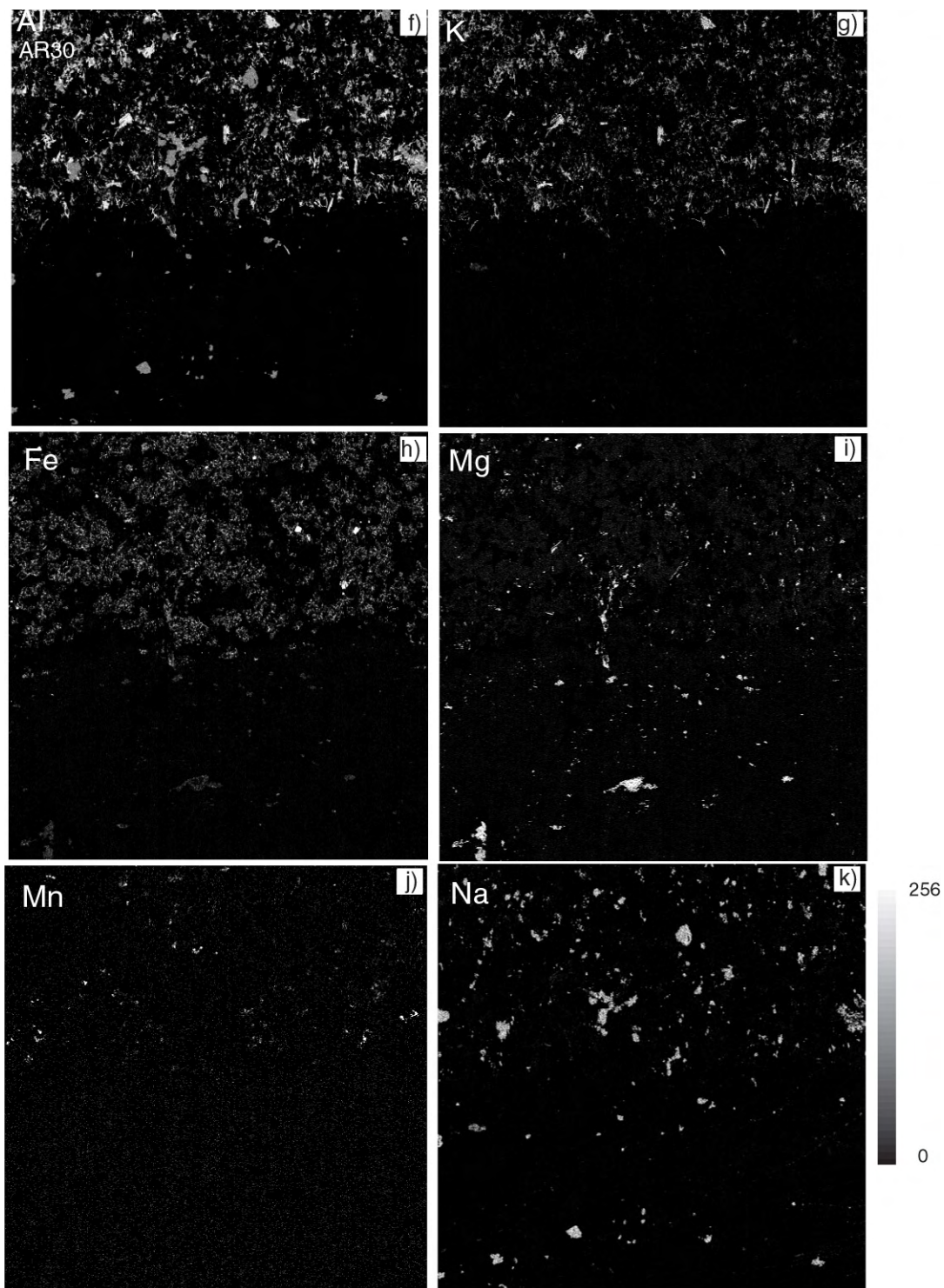


Fig. 16. Continued



#### 6.4. Cathodoluminescence (CL)

Calcite grains in both vein types have a uniform dull luminescence under CL. By contrast, quartz grains in both the rim and host luminescence more brightly than the calcite (Fig. 17b and d). Vein quartz grains in calcareous sandstone show zoning and have brighter color than one in host rock. Therefore, the CL shows no strong evidence of crystal zonation and episodic crystal growth. However, although Fe contents are below detection in both veins, CL zonation need not be visible due to lack of an activator such as Mn (Marshall, 1988).

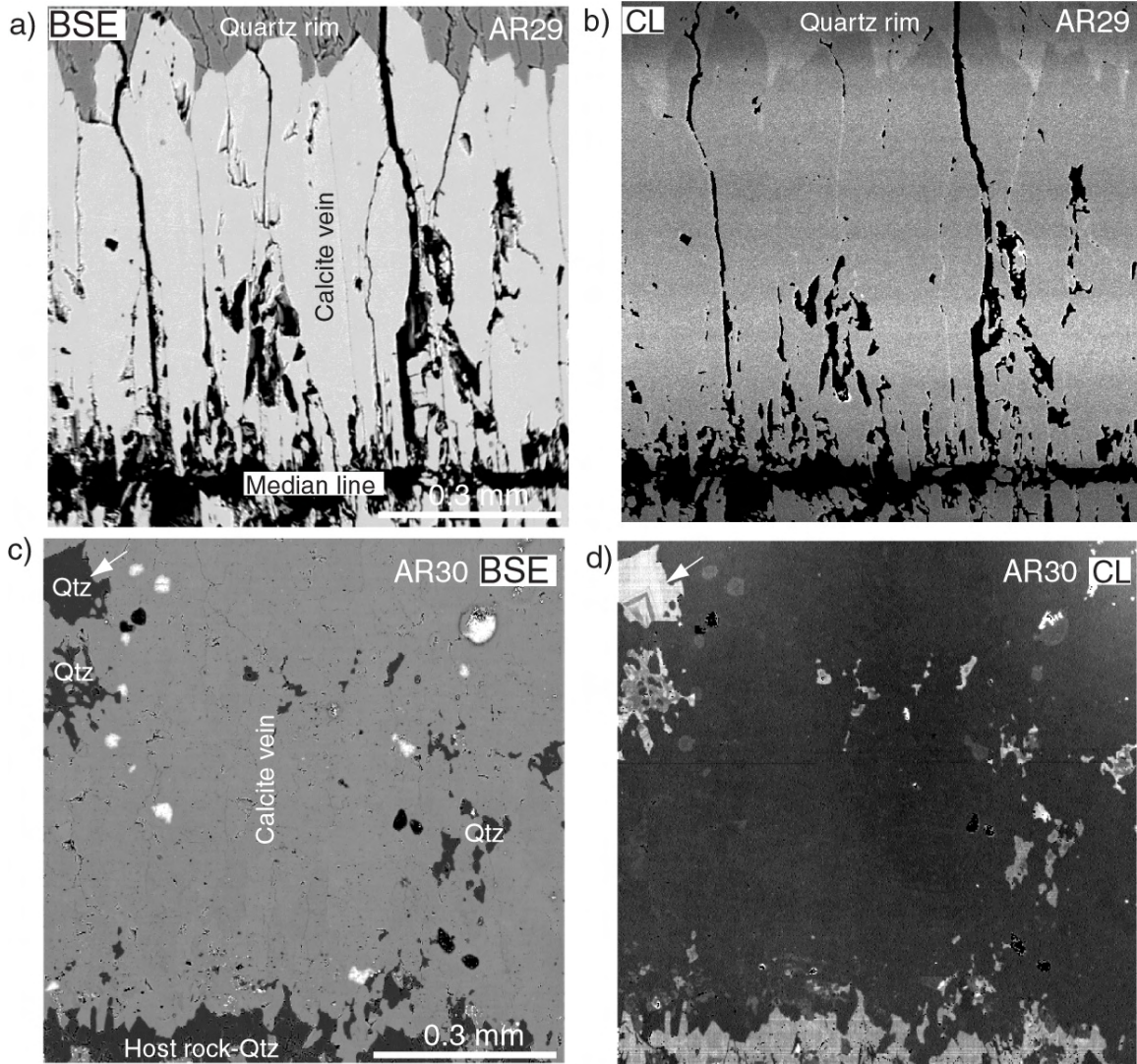


Fig. 17. Cathodoluminescence (CL) of two samples. a)-b) vein-in-shale located on Figure 10 a). c)-d) N7E vein located on Figure 14 a). The white horizontal bands in b) are scan rate artifacts. No zonation within the vein is visible in either sample. Vein quartz in sample AR30, indicated by the arrow in d), shows zonation and is brighter than quartz grains in the host. Qtz: quartz.

## 7. ISOTOPIC COMPOSITIONS

The stable isotope data are presented in the Appendix B. The analyses were performed on a Finnigan MAT 251 mass spectrometer. NBS-19 carbonate standard ( $\delta^{13}\text{C} = 1.95\text{‰}$  and  $\delta^{18}\text{O} = -2.20\text{‰}$ ) was used to calibrate  $\delta^{13}\text{C}$  and  $\delta^{18}\text{O}$  values to the Pee Dee belemnite (PDB) standard (VPDB; Coplen et al., 1996). The  $\delta^{13}\text{C}$  and  $\delta^{18}\text{O}$  values of each vein and carbonate host rock are plotted in Fig. 18 and 19.

### 7.1. Results

Veins-in-shale, N7E veins, and the blocky quartz-calcite vein show similar  $\delta^{13}\text{C}$  values (-1.9 to 1.5 ‰), whereas those of the N45E veins are lower (-2.0 to -1.6 ‰). The calcite-rich layer (CRL) has similar  $\delta^{13}\text{C}$  values to the N7E veins and the blocky quartz-calcite vein. These values are higher than those in the calcite-poor layers (CPL) and N45E veins (Fig. 19).

In contrast to the dispersion in  $\delta^{13}\text{C}$  values, the vein  $\delta^{18}\text{O}$  values are similar to each other but different in some instances from the adjacent host rock. For host rock,  $\delta^{18}\text{O}$  values of the calcite-poor layers (-10.0 to -7.8 ‰) are similar to those of calcareous sandstone containing N45E veins (-10.2 to -7.2 ‰), and they are higher than both those of N7E (I and II) veins (-13.9 to -13.5 ‰) and calcite-rich layers (-13.9 to -12.1 ‰). While N7E veins (I and II) show similar  $\delta^{18}\text{O}$  values to enclosing calcite-rich layer, N7E vein (I) has more negative  $\delta^{18}\text{O}$  values than enclosing calcite-poor layer.

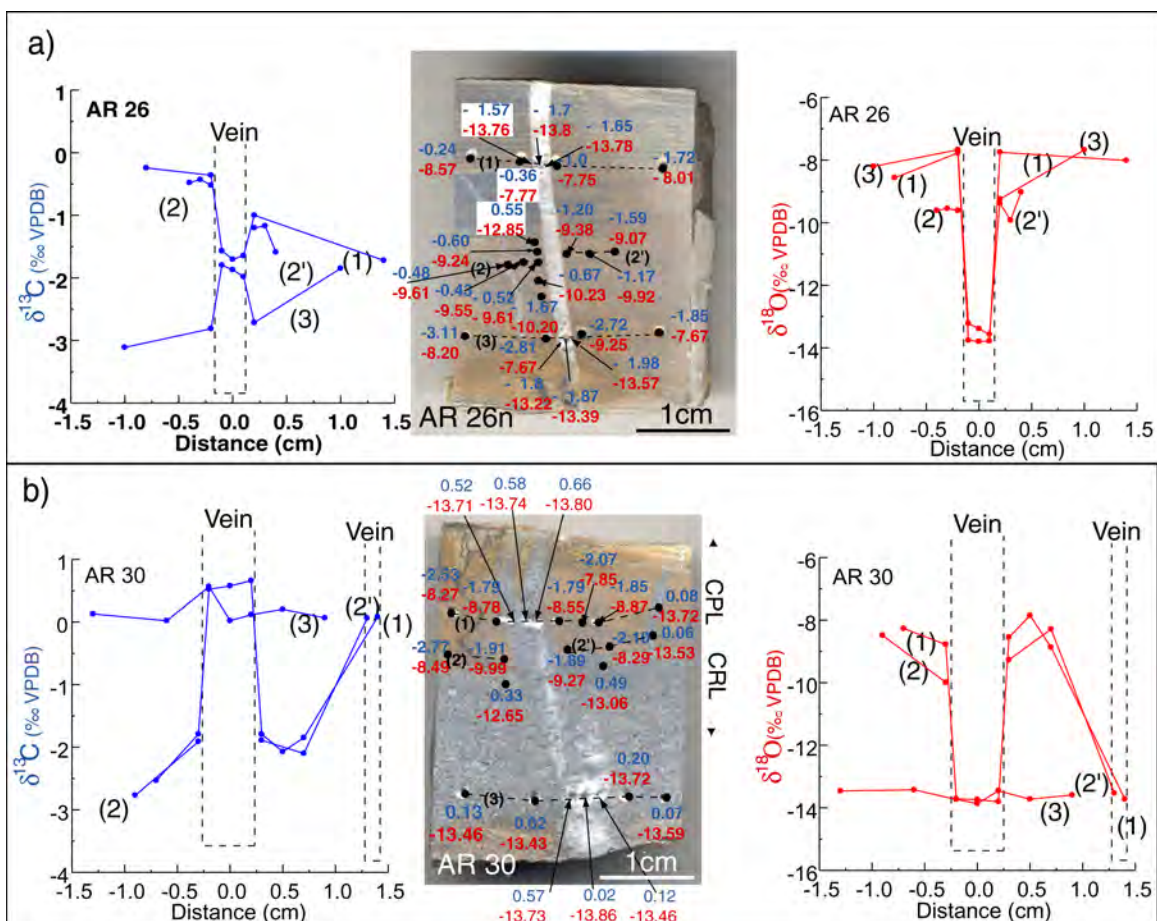


Fig. 18.  $\delta^{13}\text{C}$  and  $\delta^{18}\text{O}$  profiles across a) a N45E vein (AR 26n), b)-c) a N7E vein (AR 23 and AR 30), d) veins-in-shale (AR 29 and AR61), e) Quartz-calcite layer (AR24). a)-c)  $\delta^{13}\text{C}$  values of N45E vein and N7E vein in the calcite poor layer (CPL) are heterogeneous to their host rocks, while the  $\delta^{13}\text{C}$  values of N7E in the calcite rich layer (CRL) are similar to those of enclosing host rock. The  $\delta^{18}\text{O}$  values of N45E vein and N7E vein in the CPL are more depleted than those of their host rock, while the vein  $\delta^{18}\text{O}$  values of N7E vein in CRL are similar to those of host rock. On figures of specimens,  $\delta^{13}\text{C}$  values shown above  $\delta^{18}\text{O}$  values. CC: calcite.

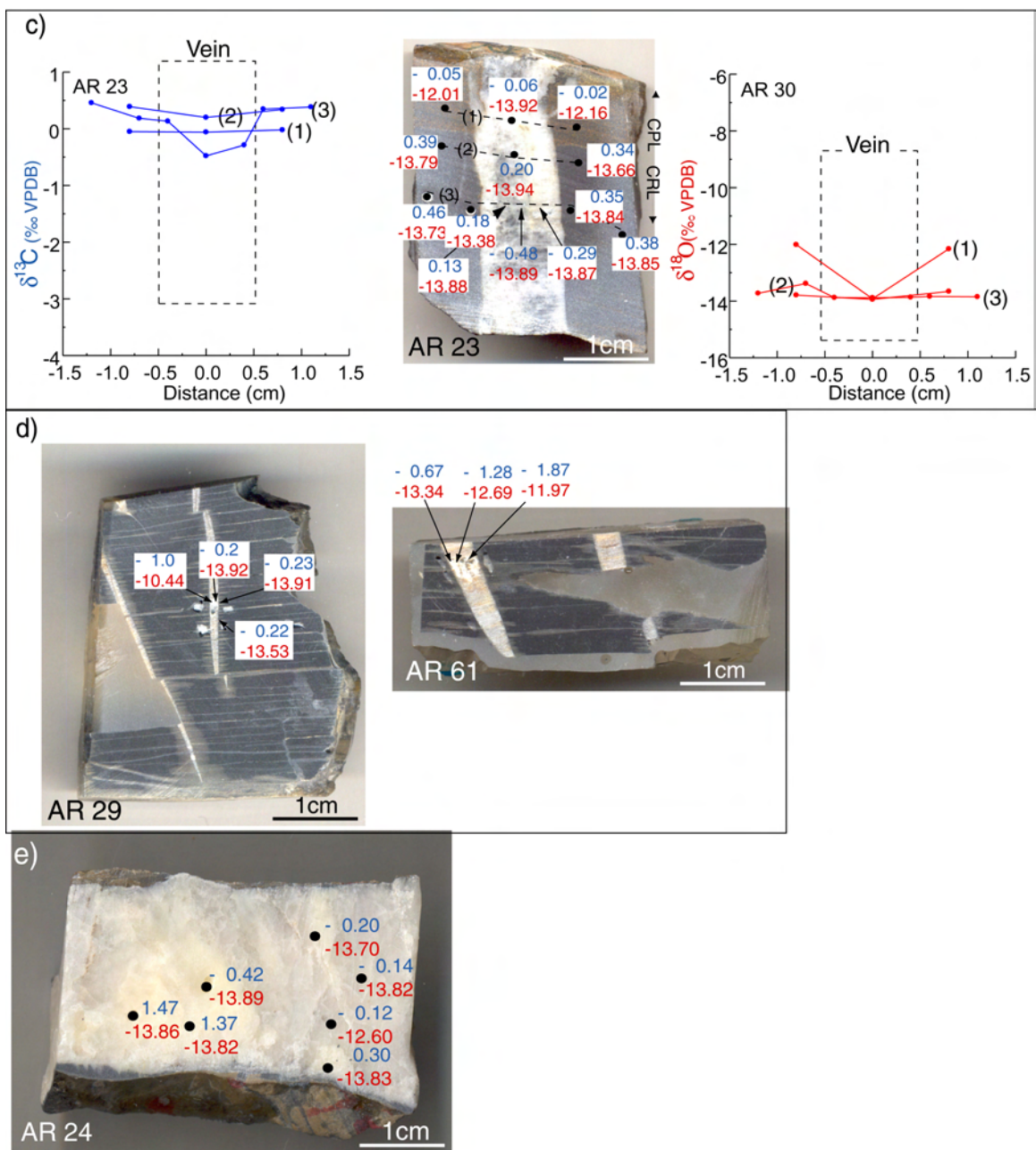


Fig. 18. Continued.



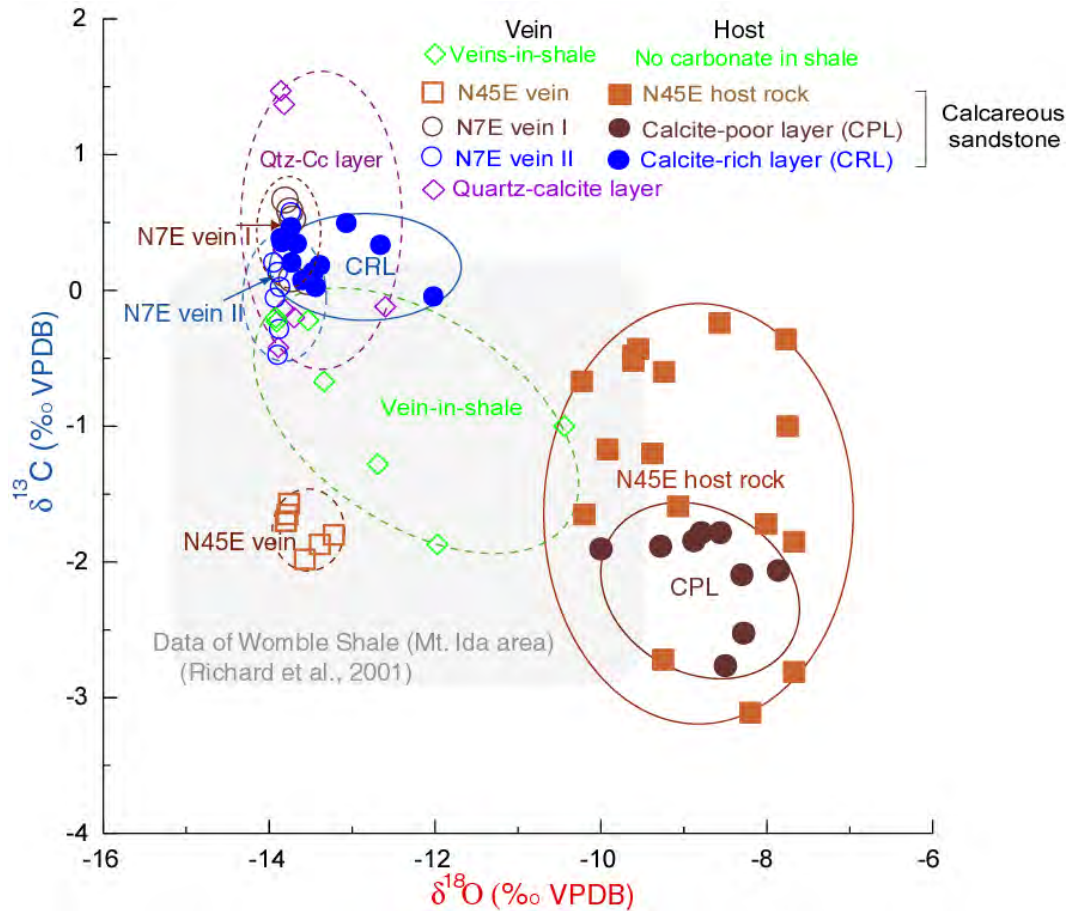


Fig. 19. Carbon and oxygen isotopic composition of veins and their host rocks. See text for details.

## 7.2. Interpretation

Similar  $\delta^{13}\text{C}$  and  $\delta^{18}\text{O}$  values between N7E veins and calcite-rich layers indicate that the calcite in veins have been derived from this host rock (path a in Fig. 20 stage 3). Even though the adjacent host for each vein may have different isotopic values, all vein types display relatively uniform carbon and oxygen isotope values close to those of the calcite-rich layers in samples AR 23 and AR 30. This fact suggests that the vein-forming fluid was in isotopic equilibrium with the calcite-rich layers, and moved into other calcareous sandstone and shale layers (path b in Fig. 20 stage 3).

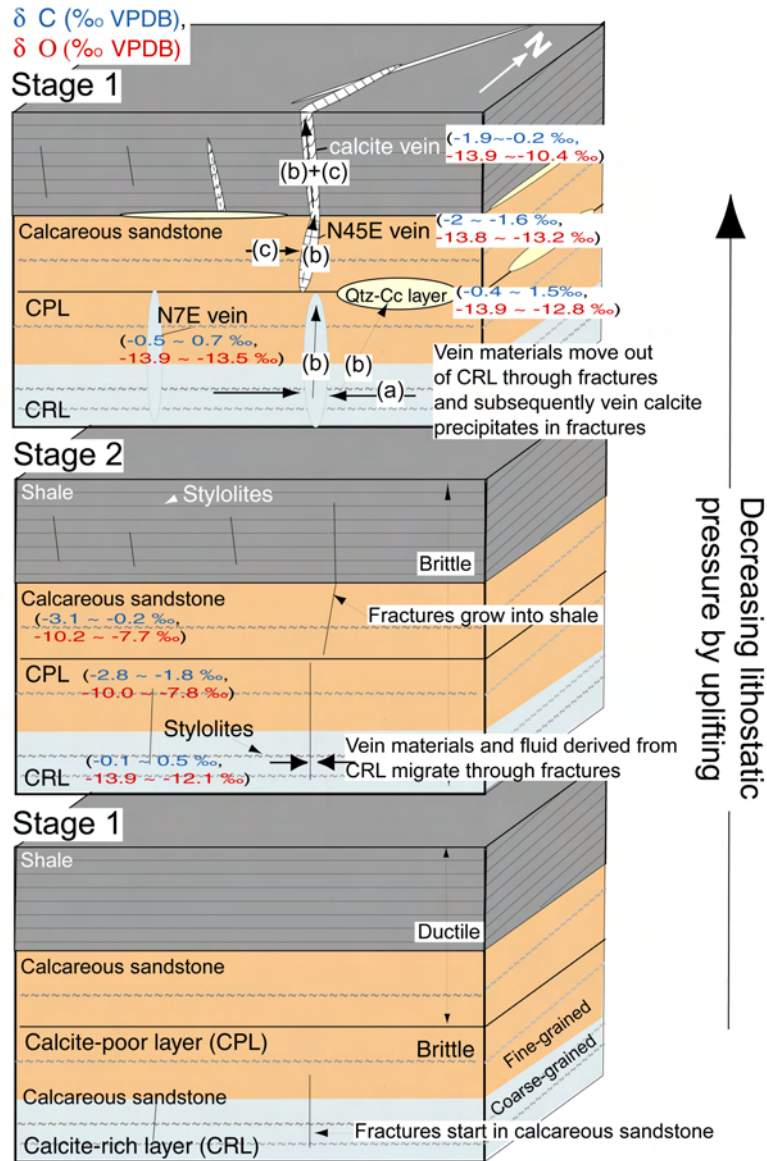


Fig. 20. Proposed diagrams illustrating the development of vein formations during uplifting, and carbon and oxygen stable isotopic relationship between veins and host rocks, and schematic fluid flow path. Stage 1: fractures develop in brittle calcareous sandstone during tectonic compression, while shale behaves more ductilely that restricts fracture growth. Stage 2: shale was probably fractured when it was brought closer to the surface by tectonic uplifting. Stage 3: (a) N7E vein-forming solution is derived from the host rock. (b) The solution of vein-forming material flows into N45E veins and veins-in-shale and quartz-calcite layer. (c) During N45E vein precipitation, the input of lower  $\delta^{13}C$  from calcareous sandstone containing N45E vein leads to depleted carbon isotope values of N45E veins relative to other veins. Carbon isotope of veins in shale might be partially mixed with this lower  $\delta^{13}C$  of the calcareous sandstone containing N45E veins.

## 8. DISCUSSION

Based on stable isotope data, all types of veins were formed by fluids in equilibrium with the calcareous sandstone beds rather than fluids derived from their adjacent host rock. Here, fractures and stylolites were likely locally interconnected and were material transfer conduits. Lower carbon isotope values of N45E veins relative to other veins suggest that input of  $^{13}\text{C}$ -depleted carbon in the enclosing host rock during N45E veins precipitation (path c in Fig. 20 stage 3), while maintaining lower oxygen isotope values.

Mineralogical and geochemical data show that veins-in-shale of the study area consist of calcite, but that calcium in the host rock is rare. The paucity of Ca in the shale suggests that either the shale itself did not supply calcite for vein or that it has all been removed; the former is the simplest explanation, especially in light of no evidence of pervasive dissolution and recrystallization. Although the permeability of Womble shale is unknown, it is reported that typical shales have very low permeability ( $10^{-17} \text{ m}^2 \sim 10^{-23} \text{ m}^2$ ; Magara, 1978; Neglia, 1979; Domenico, and Schwartz, 1990; Gutierrez et al., 2000). Low permeability of shales and little calcium content in its composition from this study indicate that calcium seems not to move through porous matrix. Based on the fact that veins-in-shale are connected with N45E vein in the outcrop, and there is the concentration of calcite within stylolites in calcium-poor shale under microprobe analysis, I interpret that calcite grains were externally derived through the interconnected fracture-stylolites system in the shale and they precipitated in the veins and stylolites.



### *8.1. Fractures and vein-filling fluid generation during tectonic compression*

The stereonet plots in Fig. 6 show the N-S trending N7E veins are syntectonic veins that most likely dilated during regional thrust-fold events. In contrast, I suggest that N45E veins and veins in shale form later than the N7E veins because of the following three reasons. 1) They trend obliquely to the transport direction, which may be the result of local change of stress field at different times, and 2) calcareous sandstone with less clay content is likely more brittle than shale at depth (Fig. 20 stage 1). After fractures first formed in calcareous sandstone, shale was likely fractured later when it was brought closer to the surface during tectonic compression that accompanies uplift of rocks (Fig. 20 stage 2). 3) Calcite-rich layers (CRL) of calcareous sandstone containing N7E veins is the source rock for all vein materials, so fractures in calcareous sandstone should be filled first to form N7E veins. Subsequently, N45E veins and veins-in-shale might be filled and form later (Fig 20 stage 3).

During tectonic compression, vein mineral and fluid in calcite-rich layers have likely been squeezed out and accommodated by excess materials of host mineral that resulted from dissolution of the host rock. Physical evidence for dissolution is seen as the stylolites in host. Stylolites in calcareous sandstone were sites of calcite dissolution whereas stylolites in shale were fluid pathways. The pore fluid from the surrounding rock would flow into fractures by differential pressure ( $\Delta P$ ) between fluids in the matrix and in the crack (Etheridge et al. 1983; Fisher and Brantley, 1992). Consequently this released fluid would move upwards by fluid buoyancy (Nakashima, 1995) or by seismic pumping (Sibson et al., 1975). At the same stage, the calcite-poor layers (CPL) with finer matrix

might have produced less pore fluid and material than the calcite-rich layers. In this scenario, vein material was transferred into open fractures. Thus, the veins are local redistribution sites of elements dissolved along stylolites during rock deformation.

## 8.2. Mass transfer models

The mass transfer mechanisms can be evaluated for veins in this study. The material for calcite veins could have transferred by: 1) advection of fluid through pores and fractures, and 2) diffusion through static pore fluid filling pore spaces. Effective transport distance by advection ( $X_a$ ) and diffusion ( $X_d$ ) may be estimated by (Fletcher and Hoffmann, 1974),

$$X_a = \frac{K\Delta P}{\eta_w \phi D} t \quad (3)$$

$$X_d = \sqrt{2D_f \phi \tau t} \quad (4)$$

where  $K$  is matrix permeability,  $\Delta P$  is pressure difference between dissolution site (rock) and precipitation site (fracture),  $\eta_w$  ( $10^{-10}$  MPa s) is viscosity of water,  $\phi$  is matrix porosity,  $D$  is crack spacing,  $t$  is time,  $D_f$  is diffusion coefficient through pore fluid, and  $\tau$  is tortuosity defined as the true path length per unit length of sample.  $\Delta P$  can be estimated to be 16 MPa/km that is derived from the differential density between rock (26 MPa/km) and fracture-filling fluid (10 MPa/km). From Eq. (3) and (4), critical time ( $t_{crit}$ ), which is defined as the time at  $X_a = X_d$ , can be calculated as (Fisher and Brantley, 1992):

$$t_{crit} = 2D_f \eta_w^2 \frac{\phi^3}{K^2} \left( \frac{D}{\Delta P} \right)^2 \quad (5)$$

Diffusion is the dominant mass transport mechanism over advection before the critical time, while advection overcomes diffusion for long distance transport after the critical time (Fig. 21a; Fletcher and Hoffmann, 1974; Etheridge et al., 1984; Fisher and Brantley, 1992; Lagasa, 1998).

To estimate each critical time ( $t_{crit}$ ) of each rock layer, I assume that  $D$  is 1 cm for veins in rock layers,  $\Delta P$  is 0.001-0.1 MPa for the vertical dimension (6 cm – 6 m) of fractures,  $K$  is  $10^{-21}$  m<sup>2</sup> for shale,  $10^{-18}$  m<sup>2</sup> for CPL and calcareous sandstone containing N45E veins, and  $10^{-17}$  m<sup>2</sup> for CRL (Domenico and Schwartz, 1990),  $D_f$  is  $10^{-8}$  m<sup>2</sup>/s (Rutter, 1976) and  $\phi$  is 0.01 for shale, 0.05 for CPL and calcareous sandstone containing N45E veins, and 0.1 for CRL (Domenico and Schwartz, 1990)(Table 2). From Eq. 5, estimated critical time can be estimated to be  $10^{-1}$ - $10^3$  years for shale,  $10^{-5}$ - $10^{-1}$  years for CPL and calcareous sandstone containing N45E veins, and  $10^{-6}$ - $10^{-2}$  years for CRL (Fig. 21b). The critical time of CRL is always  $10^5$  times as fast as that of shale at any  $\Delta P$  (Table 2). This indicates that as the time exceeds the critical time of CRL, advection is the main mass transfer in CRL, while diffusion is still dominant in shale.

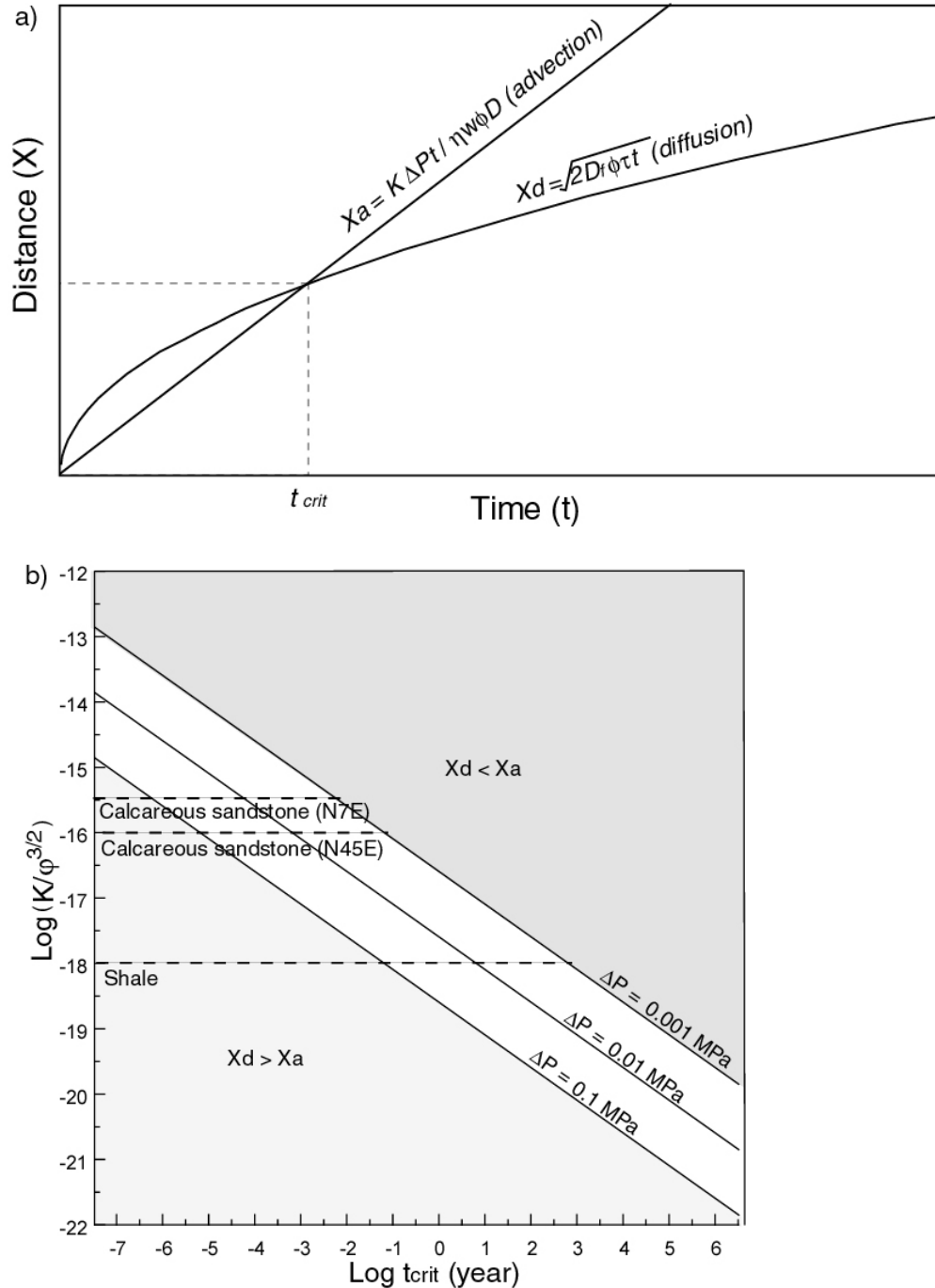


Fig. 21. a) Schematic effective transport distance of advection ( $X_a$ ) vs. diffusion ( $X_d$ ). Before  $t_{crit}$  (critical time defined as the time as  $X_a = X_d$ ), diffusion is main transport mechanism of material for shorter distance. After  $t_{crit}$ , advection is dominant mass transfer mechanism over diffusion for longer distance. b) Plot showing dependence of critical time ( $t_{crit}$ ) on the ratio ( $K/\phi$ ) of permeability to porosity of each rock layer as a function of pressure gradient ( $\Delta P$ ).

Table 2. Values of permeability ( $K$ ), pressure gradient ( $\Delta P$ ), porosity ( $\phi$ ), and calculated critical times ( $t_{crit}$ ) for rock layers. CS: Calcareous sandstone, CRL: Calcite-rich layer, CPL: Calcite-poor layer.

| Rock  | $K$ ( $m^2$ ) | $\Delta P$ (MPa) | $\phi$ | $t_{crit}$ (years)   | $t_{crit}$ ratio of CRL to each rock layer |
|-------|---------------|------------------|--------|----------------------|--|
| CRL   | $10^{-17}$    | 0.1              | 0.1    | $6.5 \times 10^{-7}$ | 1  |
|       |               | 0.01             |        | $6.5 \times 10^{-5}$ |  |
|       |               | 0.001            |        | $6.5 \times 10^{-3}$ |  |
| CS    | $10^{-18}$    | 0.1              | 0.05   | $8 \times 10^{-6}$   | >10  |
|       |               | 0.01             |        | $8 \times 10^{-4}$   |  |
|       |               | 0.001            |        | $8 \times 10^{-2}$   |  |
| Shale | $10^{-21}$    | 0.1              | 0.01   | $6.5 \times 10^{-2}$ | $10^5$                                     |
|       |               | 0.01             |        | 6.5                  |  |
|       |               | 0.001            |        | $6.5 \times 10^{-2}$ |  |

Although small veins can form by diffusion, it may be difficult to form larger veins in this manner because of the limited vein-forming material around veins and low diffusion coefficient (Cartwright and Buick, 2000). Within a particular time after the critical time of CRL, the mass-solution from CRL by advection can be more transported to fill fractures than the material from other rock layer by diffusive transport. Consequently, excess mass-solution from CRL would move into fractures in other rock layers. This assumption from different rock properties is why vein materials would be derived from CRL. During this stage, silica diffused from the shale was likely precipitated as quartz rim in veins-in-shale. The diffusive mass transfer model proposed by Fisher et al. (1995) implies locally derived calcite and requires the calcite depletion zones in the wall rock adjacent to the side of vein growth. However, in N7E veins and their host rock samples from Mt. Ida, Arkansas, there is no Ca depletion halo in wall rock boundaries adjacent to veins. It indicates that calcite contained within the veins was advectively transported from a source other than the adjacent wall rock and material migration into veins was much faster than vein crystal growth.

### *8.3. Fibrous vein formation*

Vein fibers in the fine matrix have higher length-to-width ratio than in coarser fractions. While narrower vein fibers are found in a finer matrix, longer vein fibers develop in wider vein rather than matrix size. Both vein fiber's width and vein aperture are the critical factors in controlling fibrous ratio of vein fiber. Hilgers et al. (2001) proposed that high amplitude wall rock irregularities and long wavelength wall rock

roughness lead to larger fiber width. Inversely, narrow fibers develop, in their views, from veins walls that are either smooth or display high-frequency roughness. However, the model of Hilgers et al. (2001) is not easily tested in the case of Mt. Ida veins, because it is difficult to clearly define the wall shape and identify how fibers contact on wall in N7E veins.

$\delta^{13}\text{C}$  and  $\delta^{18}\text{O}$  profiles across N7E veins and host rock reveal that there is no significant isotopic variation across a single vein (Fig. 18 a, b, and c). Textures observed under cathodoluminescence (CL) also indicate that the zonation patterns are uniform in veins. Therefore, there is no strong evidence for multiple and discrete crack-seal events of fibrous veins. The development of these veins need not be by a repeated opening-sealing processes. The same fluid was involved in all stages of vein formation.

The force of crystallization can be still possible mechanism of a fibrous vein formation, only if supersaturation of vein-filling solution is maintained in the system and moves along fracture and stylolites. Although quartz vein in slate may result from the diffusion as Fisher and Brantley (1992) and Fisher et al. (1995) proposed, the diffusion model does not fit fibrous calcite veins-in-shale. This study suggests that fibrous vein formation relate with Ouachita orogeny and advection model is more applicable to calcite veins-in-shale. This is consistent with Ramsay and Huber (1983)'s assumption that calcite in 'antitaxial' veins in shale was probably transported from local carbonate rocks under centimeter to meter scale.

## 9. CONCLUSION

1. Calcite veins-in-shale show 'antitaxial texture, and N45E veins and N7E veins in calcareous sandstone have the features of 'stretched' veins. The N-S trending N7E veins in calcareous sandstone are syntectonic veins formed during Paleozoic Ouachita orogeny.
2. Calcite vein fibers that are subnormal to walls of the vein are more fibrous (high length to width ratio) in a finer matrix, showing that vein fiber width decreases as host grain size decreases.
3. No zoning in cathodoluminescence or stable isotopes was observed in the veins, suggesting there is no clear evidence for diffusion from the host to the vein.
4. Carbon and oxygen isotope data from veins are identical to those of local calcite-rich layers in calcareous sandstone. The wide variety of veins was probably formed from meter-scale migration of fluid derived from local calcite-rich layers in calcareous sandstone.



## REFERENCES

- Arbenz, J. K., 1984. A structural cross section through the Ouachita Mountains of western Arkansas. In: Stone, C. G., Haley, B. R., (Eds), A guidebook to the geology of the central and southern Ouachita Mountains, Arkansas, Little Rock, Arkansas Geological Commission Miscellaneous Publication, pp. 76-85.
- Babaei, A., and Viele, G. W., 1992. Two-decked nature of the Ouachita Mountains, Arkansas. *Geology* 20, 995-998.
- Blythe, A. E., Sugar, A., Phipps, S. P., 1988. Structural profiles of Ouachita Mountains, western Arkansas. *American Association of Petroleum Geologists Bulletin* 72, 810-819.
- Cartwright, I., Buick, I. S., 2000. Fluid generation, vein formation and the degree of fluid-rock interaction during decompression of high-pressure terranes: the Schistes Lustrés, Alpine Corsica, France. *Journal of Metamorphic Geology* 18, 607-624.
- Coplen, T. B., De Bievre, P., Krouse, H. R., Vock, D., Groning, Jr., M., and Rozanski, K., 1996. Ratios for light element isotopes standardized for better interlaboratory comparison. *Eos* 77, 255.
- Cox, S.F., Etheridge, M.A., 1983. Crack-seal fibre growth mechanisms and their significance in the development of oriented layer silicate microstructures. *Tectonophysics* 92, 147-170.
- Dewers, T., Ortoleva, P., 1990. Force of crystallization during the growth of siliceous concretions, *Geology* 18, 204-207.
- Domenico, P. A., Schwartz, F. W., 1990. *Physical and chemical hydrogeology*, John Wiley and Sons, New York, 824pp.
- Durney, D.W., Ramsay, J.G., 1973. Incremental strains measured by syntectonic crystal growths. In: DeJong, K.A. and Scholten, R.(Eds), *Gravity and tectonics*, John Wiley and Sons, New York, pp. 67-96.
- Elliott D., 1973. Diffusion flow laws in metamorphic rocks. *Geological Society of America Bulletin* 84, 2645-2664.
- Etheridge, M. A., Wall, V. J., Vernon, R. H., 1983. The role of the fluid phase during regional metamorphism and deformation. *Journal of Metamorphic Geology*. 1, 205-226.

- Etheridge, M.A., Wall, V.J., Cox, S.F. and Vernon, R.H., 1984. High fluid pressures during regional metamorphism and deformation: implications for mass transport and deformation mechanisms. *Journal of Geophysical Research* 89, 4344-4358.
- Fisher, D.M., Brantley, S.L., 1992. Models of quartz overgrowth and vein formation; deformation and episodic fluid flow in an ancient subduction zone. *Journal of Geophysical Research* 97, 20043-20061.
- Fisher, D.M., Brantley, S.L., Everett, M. and Dzvoniak, J., 1995. Cyclic flow through a regionally extensive fracture network within the Kodiak accretionary prism. *Journal of Geophysical Research* 100, 12881-12894.
- Fletcher, R. C., Merino, E., 2001. Mineral growth in rocks: Kinetic-rheological models of replacement, vein formation, and syntectonic crystallization. *Geochimica et Cosmochimica Acta.* 65, 3733-3748.
- Gray, D. R., Gregory, R. T., 1991. Rock-buffered fluid interaction in deformed quartz-rich turbidite sequence, eastern Australia. *Journal of Geophysical Research* 96, 19681-19704.
- Haley, B. R., and Stone, C., 1976. CoGeo map of Arkansas: U.S. Geological Survey and Arkansas Geological Commission, scale 1:24,000.
- Henry, C., Burkhard, M., Goffé, B., 1996. Evolution of synmetamorphic veins and their wallrocks through a Western Alps transect: no evidence for large-scale fluid flow. Stable isotope, major- and trace-element systematics. *Chemical Geology* 127, 81-109.
- Hilgers, C., Koehn, D., Bons, P. D., Urai, J. L., 2001. Development of crystal morphology during uniaxial growth in a progressively widening vein: II. Numerical simulations of the evolution of antitaxial fibrous veins. *Journal of Structural Geology* 23, 873-885.
- Houseknecht, D. W., Mattews, S. M., 1985. Thermal maturity of carboniferous strata, Ouachita Mountains. *American Association of Petroleum Geologists* 69, 335-345.
- Howard, J. M and Stone, C., 1988, Quartz crystal deposits of the Ouachita Mountains, Arkansas and Oklahoma. *Arkansas Geological Commission Miscellaneous Publication*, pp. 63-71.
- Kirschner, D. L., Sharp, Z. D., Masson, H., 1995. Oxygen isotope thermometry of quartz-calcite veins; Unveiling the thermal-tectonic history of the subgreenschist facies Morcles nappe (Swiss Alps). *Geological Society of American Bulletin* 107, 1145-1156.

- Lasaga, A. C., 1998. Kinetic theory in the earth sciences, Princeton University Press. Princeton, New Jersey, 811pp.
- Li T., 2000. Experimental growth of fibers and fibrous veins. Ph.D. dissertation, State University of New York at Albany.
- Lillie, R. J., Nelson, K. D., DeVoogd, B., Brewer, J. A., Oliver, J. E., Brown, L. D., Kaufman, S., Viele, G. W., 1983. Crustal structure of Ouachita Mountains, Arkansas: a model based on integration of COCORP reflection profiles and regional geophysical data. American Association of Petroleum Geologists Bulletin 67, 907-931.
- Maliva R., Siever, R., 1988. Mechanism and controls of silicification of fossils in limestone. The Journal of Geology 96, 387-397.
- Marshall, D. J., 1988. Cathodoluminescence of geological materials, Allen and Unwin, Boston, 146pp.
- McFarland, J. D., 1998. Stratigraphic summary of Arkansas. Arkansas Geological Commission. Little Rock, Arkansas. 36, 39pp.
- Means, W. D., and Li, 2001. A laboratory simulation of fibrous veins: some first observations. Journal of Structural Geology 23, 857-863.
- Miser, H. D., 1959, Structure and vein quartz of the Ouachita Mountains of Oklahoma and Arkansas. In: The geology of the Ouachita Mountains, a symposium: Dallas and Ardmore Geological Societies, pp. 30-43
- Nicolis, G., Prigogine, I., 1977. Self-organization in non-equilibrium systems, Wiley, New York, 491pp.
- Pitt, W. D., Cohoon R. R., Lee, H. C., Robb, M. G., Watson, J., 1961. Ouachita Mountain core area, Montgomery County, Arkansas. Bulletin of the American Association of Petroleum Geologists 45, 72-94.
- Ramsay, J.G., 1980. The crack-seal mechanism of rock deformation. Nature 284, 135-139.
- Ramsay, J.G., Huber, M., 1983. The Techniques of modern structural geology, Volume. 1: Strain Analysis, Academic Press, London, 307pp.
- Richard, I. J., Connelly, J. B., Gregory, R. T., Gray, D. R., 2002. The importance of diffusion, advection, and host-rock lithology in vein formation: A stable isotope study from the Paleozoic Ouachita orogenic belt, Arkansas and Oklahoma. Geological Society of America Bulletin 114, 1342-1355.

- Rutter, E. H., 1976. The kinetics of rock deformation by pressure solution. *Philosophical Transactions of the Royal Society of London*. 283, 203-219.
- Rye, D., Bradbury, H. J., 1988. Fluid flow in the crust; an example from a Pyrenean thrust ramp. *American Journal of Science* 288, 197-235.
- Sibson, R. H., Moore, J. M., Rankin, A. H., 1975. Seismic pumping—a hydrothermal fluid transport mechanism. *Journal of Geological Society London* 131, 653-659.
- Stone, C, and Sterling, P., 1962. New lithologic marker horizons in Ordovician rocks, eastern Ouachitas of Arkansas, *Bulletin of the American Association of Petroleum Geologists* 46, 387-390.
- Taber, S., 1916a. The growth of crystals under external pressure. *American Journal of Science* 41, 532-556.
- Taber, S., 1916b. The origin of veins in asbestiform minerals. *Proceedings of the National Academy of Sciences* 2, 659-664.
- Taber, S., 1917. The genesis of asbestos and asbestiform minerals. *Transactions of the American Institute of Mining and Engineering* 57, 67-98.
- Viele, G. W., 1973. Structure and tectonic history of the Ouachita Mountains, Arkansas, in *Gravity and Tectonics*: New York, John Wiley. 361-377.
- Viele G. W., Thomas, W. A., 1989. Tectonic synthesis of the Ouachita orogenic belt. In Hatcher, R. D., Jr., Thomas, W. A., Viele, G. W., (Eds), *The Appalachian-Ouachita orogen in the United States The Geology of North America*, Geological Society of America F-2, Boulder, Colorado, pp. 695-728.
- Wiltschko, D.V., 1998. Chapters by Wiltschko in *Analysis of Veins in Low Temperature Environments—Introduction for Structural Geologists*, Geological Society of America Short Course by D.V. Wiltschko, J.W. Morse, Z.D. Sharp, W.M. Lamb, Toronto, 1998.
- Wiltschko, D. V., Morse, J. W., 2001. Crystallization pressure versus "crack seal" as the mechanism for banded veins. *Geology* 29, 79-82.

## APPENDIX A

Description of samples. CS: Calcareous sandstone, Qtz-cc layer: Quartz-calcite layer

| Sample | Host  | Vein type     | Thin section |             |           |             | Analysis    |                |
|--------|-------|---------------|--------------|-------------|-----------|-------------|-------------|----------------|
|        |       |               | Number       | Orientation | Long axis | View        | Micro probe | Stable Isotope |
| AR 23  | CS    | N7E vein      | AR 23        | N45W, 87S   | Vertical  | Rock facing |             | ○              |
| AR 24  |       | Qtz-cc layer  |              |             |           |             |             | ○              |
| AR 26n | CS    | N45E vein     | AR 26n       | N85W, 70S   | Vertical  | Rock facing |             | ○              |
| AR 29  | Shale | Vein-in-shale | AR 29        | N30W, 80S   | Vertical  | Rock up     | ○           | ○              |
|        |       |               | AR 29c       | N30W, 80S   | Vertical  | Rock up     | ○           |                |
| AR 30  | CS    | N7E vein      | AR 30        | N55W, 72S   | Vertical  | Rock up     | ○           | ○              |
| AR 61  | Shale | Vein-in-shale | AR 61-1      | N70E, 10N   | N55E      | Rock facing |             |                |
|        |       |               | AR61-2       | N30W, 88S   | Vertical  | Rock up     |             | ○              |

### APPENDIX B

Mean and standard deviation values of host and vein grains of N7E vein in calcareous sandstone (AR30).

| Mineral | Matrix layer         | Host / Vein    | Mean $\pm$ Standard deviation        |                        |
|---------|----------------------|----------------|--------------------------------------|------------------------|
| Calcite | Coarse-grained layer | Host           | $0.04 \pm 0.014$ (mm <sup>2</sup> )  |                        |
|         |                      | Vein grain     | Width                                | $0.034 \pm 0.02$ (mm)  |
|         |                      |                | Length                               | $0.094 \pm 0.05$ (mm)  |
|         |                      |                | Width / length                       | $3.4 \pm 2.4$          |
|         | Fine-grained layer   | Host           | $0.005 \pm 0.003$ (mm <sup>2</sup> ) |                        |
|         |                      | Vein grain     | Width                                | $0.013 \pm 0.006$ (mm) |
| Length  |                      |                | $0.117 \pm 0.05$ (mm)                |                        |
|         |                      |                | Width / length                       | $9.4 \pm 2.4$          |
| Quartz  | Coarse-grained layer | Host           | $0.02 \pm 0.01$ (mm <sup>2</sup> )   |                        |
|         |                      | Vein grain     | Width                                | $0.043 \pm 0.024$ (mm) |
|         |                      |                | Length                               | $0.057 \pm 0.026$ (mm) |
|         |                      |                | Width / length                       | $1.5 \pm 0.65$         |
|         | Fine-grained layer   | Host           | $0.01 \pm 0.007$ (mm <sup>2</sup> )  |                        |
|         |                      | Vein grain     | Width                                | $0.019 \pm 0.016$ (mm) |
| Length  |                      |                | $0.031 \pm 0.038$ (mm)               |                        |
|         |                      | Width / length | $1.7 \pm 0.76$                       |                        |



### APPENDIX C

Carbon and oxygen stable isotopic data of host rock and veins in study area. CRL: Calcite-rich layer, CPL: Calcite-poor layer.

| Host rock/Vein                 | Sample number | Distance from mid vein (cm)<br>+/-:right/left | $\delta^{13}\text{C}$<br>(VPDB) | $\delta^{18}\text{O}$<br>(VPDB) | Remark    |
|--------------------------------|---------------|---|---------------------------------|---------------------------------|-----------|
| Calcareous sandstone/N7E vein  | AR23-1        | 1.1   | 0.38                            | -13.85                          | CRL       |
|                                | AR23-2        | 0.6   | 0.35                            | -13.84                          | CRL       |
|                                | AR23-3        | 0.4   | -0.29                           | -13.87                          | Vein      |
|                                | AR23-4        | 0   | -0.48                           | -13.89                          | Vein      |
|                                | AR23-5        | -0.4  | 0.13                            | -13.88                          | Vein      |
|                                | AR23-6        | -0.7  | 0.18                            | -13.38                          | CRL       |
|                                | AR23-7        | -1.2  | 0.46                            | -13.73                          | CRL       |
|                                | AR23-8        | -0.8  | -0.05                           | -12.01                          | CPL       |
|                                | AR23-9        | 0   | -0.06                           | -13.92                          | Vein      |
|                                | AR23-10       | 0.8   | -0.02                           | -12.16                          | CPL       |
|                                | AR23-11       | -0.8  | 0.39                            | -13.79                          | CRL       |
|                                | AR23-12       | 0   | 0.20                            | -13.94                          | Vein      |
|                                | AR23-13       | 0.8   | 0.34                            | -13.66                          | CRL       |
| Quartz-Calcite layer           | AR24-1        |   | 1.47                            | -13.89                          |           |
|                                | AR24-2        |   | -0.42                           | -13.89                          |           |
|                                | AR24-3        |   | -0.12                           | -12.60                          |           |
|                                | AR24-4        |   | 1.37                            | -13.82                          |           |
|                                | AR24-5        |   | 0.30                            | -13.83                          |           |
|                                | AR24-6        |   | -0.14                           | -13.82                          |           |
|                                | AR24-7        |   | -0.20                           | -13.70                          |           |
| Calcareous sandstone/N45E vein | AR26-1        | 1.0   | -1.85                           | -7.67                           | Host rock |
|                                | AR26-2        | 0.2   | -2.72                           | -9.25                           | Host rock |
|                                | AR26-3        | 0.1   | -1.98                           | -13.57                          | Vein      |
|                                | AR26-4        | 0   | -1.87                           | -13.39                          | Vein      |
|                                | AR26-5        | -0.1  | -1.80                           | -13.22                          | Vein      |
|                                | AR26-6        | -0.2  | -2.81                           | -7.67                           | Host rock |
|                                | AR26-7        | 1   | -3.11                           | -8.20                           | Host rock |
|                                | AR26-8        | 1.4   | -1.72                           | -8.01                           | Host rock |
|                                | AR26-9        | 0.2   | -1.00                           | -7.75                           | Host rock |
|                                | AR26-10       | 0.1   | -1.65                           | -13.78                          | Vein      |
|                                | AR26-11       | 0   | -1.70                           | -13.80                          | Vein      |
|                                | AR26-12       | -0.1  | -1.57                           | -13.76                          | Vein      |
|                                | AR26-13       | -0.2  | -0.36                           | -7.77                           | Host rock |
|                                | AR26-14       | -0.8  | -0.24                           | -8.57                           | Host rock |
|                                | AR26-15       | -0.2  | -1.65                           | -10.20                          | Host rock |
|                                | AR26-16       | -0.2  | -0.67                           | -10.23                          | Host rock |
|                                | AR26-17       | -0.2  | -0.52                           | -9.61                           | Host rock |
|                                | AR26-18       | -0.3  | -0.43                           | -9.55                           | Host rock |
|                                | AR26-19       | -0.4  | -0.48                           | -9.61                           | Host rock |

|                                  |           |      |       |        |           |
|----------------------------------|-----------|------|-------|--------|-----------|
|                                  | AR26-20   | 0.2  | -1.20 | -9.38  | Host rock |
|                                  | AR26-21   | 0.3  | -1.17 | -9.92  | Host rock |
|                                  | AR26-22   | 0.4  | -1.59 | -9.07  | Host rock |
|                                  | AR26-23   | -0.2 | -0.60 | -9.24  | Host rock |
|                                  | AR26-24   | -0.2 | 0.55  | -12.85 | Host rock |
| Shale/Fibrous vein               | AR29-3    | 1.0  | -1.00 | -10.44 | Vein      |
|                                  | AR29-4    | 0    | -0.20 | -13.92 | Vein      |
|                                  | AR29-5    | -1.0 | -0.23 | -13.91 | Vein      |
|                                  | AR29-8    | 0.8  | -0.22 | -13.53 | Vein      |
| Calcareous<br>sandstone/N7E vein | AR30-1    | 0.7  | -1.85 | -13.89 | CPL       |
|                                  | AR30-2    | 0.3  | -1.79 | -13.89 | CPL       |
|                                  | AR30-3    | 0.2  | 0.66  | -12.60 | Vein      |
|                                  | AR30-4    | 0    | 0.58  | -13.74 | Vein      |
|                                  | AR30-5    | -0.2 | 0.52  | -13.71 | Vein      |
|                                  | AR30-6    | -0.3 | -1.79 | -0.87  | CPL       |
|                                  | AR30-8    | -0.7 | -2.53 | -8.27  | CPL       |
|                                  | AR30-9    | 0.9  | 0.07  | -13.59 | CRL       |
|                                  | AR30-10   | 0.5  | 0.20  | -13.72 | CRL       |
|                                  | AR30-10-1 | 0.2  | 0.12  | -13.46 | Vein      |
|                                  | AR30-11   | 0    | 0.02  | -13.86 | Vein      |
|                                  | AR30-12   | -0.2 | 0.57  | -13.73 | Vein      |
|                                  | AR30-13   | -0.6 | 0.02  | -13.43 | CRL       |
|                                  | AR30-14   | -1.3 | 0.13  | -13.46 | CRL       |
|                                  | AR30-15   | -0.3 | 0.33  | -12.65 | CRL       |
|                                  | AR30-16   | 0.6  | 0.49  | 13.06  | CRL       |
|                                  | AR30-17   | 0.3  | -1.89 | -9.27  | CPL       |
|                                  | AR30-18   | 0.7  | -2.10 | -8.29  | CPL       |
|                                  | AR30-19   | 0.5  | -2.07 | -7.85  | CPL       |
|                                  | AR30-20   | -0.9 | -2.77 | -8.49  | CPL       |
|                                  | AR30-21   | -0.3 | -1.91 | -9.99  | CPL       |
|                                  | AR30-22   | 0    | 0.08  | -13.72 | Subvein   |
|                                  | AR30-23   | 0    | 0.06  | -13.53 | Subvein   |
| Shale/Fibrous vein               | AR61-1    | -1.5 | -1.87 | -11.97 | Vein      |
|                                  | AR61-2    | -1.5 | -0.67 | -13.34 | Vein      |
|                                  | AR61-3    | 0    | -1.28 | -12.69 | Vein      |

**VITA**

Name: Jae Won Chung

Born: Oct 18, 1971

Education: B.S, Geology, Yonsei University, Seoul Korea, 1996  
M.S., Geology, Seoul National University, Seoul Korea, 1998

Permanent Address: 306-602 Kunyoung APT Koyang, Kyunggi-do  
411-707, Korea